ANALYSIS OF CHANGES IN STRUCTURE AND MOISTURE IN STARCH EXTRUDATES DURING STORAGE USING MICRO-CT AND MRI IMAGING TECHNIQUES

by

CHRISTINA ALEXIS CASTLEJOHN

(Under the Direction of Louise Wicker)

ABSTRACT

The number of extruded starch products has increased in the food industry in recent years. The application of different imaging techniques, such as Microcomputed tomography (microCT) and Magnetic Resonance Imaging (MRI), can provide a better understanding of changes occurring during storage of these products. The goal of this research was to use microCT and MRI to study changes in starch extrudates during 8 weeks of storage. MicroCT found density changes in the pore network of the extrudate and detected high density areas within the solid material. The mean and median pore diameter (0.016 mm) did not change during storage. However, the pore network expanded in size and scope within the first 4 weeks of storage with an increase in the % porosity and the % pore interconnectivity as well as a flattening and widening of the pore diameter distribution. The high density areas, which were concentrated in the center of the extrudate, showed no trend during storage, and their composition is unknown. MRI was used to study changes in the moisture distribution and mobility during storage. Various methods were applied using this technique, including T2 imaging. A complex moisture pattern was seen during storage. Even though the concentration of water remained consistent throughout the extrudate, areas of high and low free water concentration were seen by Week 8 suggesting

that the areas of lower free water, found outside the center of the extrudate, contained more

bound water. In addition, the free water mobility, which was lower after 8 weeks of storage, was

higher in the center even though the highest concentration of free water was not found in the

center of the extrudate. These results show a complexity of moisture migration during storage of

starch extrudates. The results of both imaging techniques suggest a possible relationship between

the structural changes and the complexity in the moisture distribution.

INDEX WORDS:

MicroCT, X-ray tomography, Magnetic Resonance Imaging, starch,

extrusion

ANALYSIS OF CHANGES IN STRUCTURE AND MOISTURE IN STARCH EXTRUDATES DURING STORAGE USING MICRO-CT AND MRI IMAGING TECHNIQUES

by

CHRISTINA ALEXIS CASTLEJOHN

A.A., Oxford College of Emory University, 1998B.S., Georgia Institute of Technology, 2002M.S., University of Georgia, 2009

A Dissertation Submitted to the Graduate Faculty of The University of Georgia in Partial Fulfillment of the Requirements for the Degree

DOCTOR OF PHILOSOPHY

ATHENS, GEORGIA

2012

© 2012

Christina Alexis Castlejohn

All Rights Reserved

ANALYSIS OF CHANGES IN STRUCTURE AND MOISTURE IN STARCH EXTRUDATES DURING STORAGE USING MICRO-CT AND MRI IMAGING TECHNIQUES

by

CHRISTINA ALEXIS CASTLEJOHN

Major Professor: Louise Wicker Committee: John P. Shields

Rakesh K. Singh Hong Zhuang

Electronic Version Approved:

Maureen Grasso Dean of the Graduate School The University of Georgia August 2012

DEDICATION

To my family and friends, thank you for all of your encouragement. This would not have been possible without you.

ACKNOWLEDGEMENTS

I would like to thank Dr. Wicker for being my mentor and helping me navigate my way through graduate school. I would also like to thank Dr. Shields, Dr. Singh, and Dr. Zhuang for their guidance and support during this entire process. They have been of immeasurable help to me. I would also like to thank Dr. Ronald Holser and Dr. Samantha Hawkins at the USDA Russell Research Center for all of their help in the execution and planning of this research. Thankfully, Dr. Johannes Leisen and Angela Lin at the Georgia Institute for Technology both graciously allowed me to use their imaging equipment and grill them for information. Dr. George Cavender always leant me a helping hand and not only trained me in extrusion, but helped me in expanding the scope of my research. The entire Wicker lab group helped support me, but particularly Deepika Karnik and Haiqin Dong, who have become lifelong friends. Finally, I would like to thank all of the staff in the Food Science department.

TABLE OF CONTENTS

		Page
ACKNO'	WLEDGEMENTS	v
LIST OF	TABLES	viii
LIST OF	FIGURES	ix
СНАРТЕ	ER	
1	INTRODUCTION	1
	References	3
2	LITERATURE REVIEW	4
	Starch	4
	Extrusion	8
	Analytical Techniques	10
	Imaging Techniques	15
	Conclusions	20
	References	22
3	STARCH EXTRUDATE STRUCTURE MEASURED BY MICRO-CT DU	IRING
	STORAGE	46
	Abstract	47
	Introduction	48
	Materials and Methods	50
	Results and Discussion	54

	Conclusions 61
	References
4	COMPLEXITY OF CHANGES IN MOISTURE DURING STORAGE OF STARCH
	EXTRUDATES AS CHARACTERIZED BY MRI
	Abstract
	Introduction
	Materials and Methods 80
	Results and Discussion84
	Conclusions 90
	References
5	CONCLUSIONS98

LIST OF TABLES

	Page
Table 2.1: Characteristic of starch granules from different botanical sources	32
Table 2.2: Spin of nuclei used for NMR	45
Table 3.1: Ratios of crystalline to amorphous starch peaks measured by FTIR	68
Table 3.2: Summary of pore characteristics during storage	70
Table 3.3: Summary of pore characteristics at different times post-cutting during Week 4 of	
storage	72
Table 4.1: Ratios of crystalline to amorphous starch peaks measured by FTIR	95
Table 4.2: Description of methods used during MRI	97

LIST OF FIGURES

	Page
Figure 2.1: Scanning electron micrographs of starches separated from different sources	31
Figure 2.2: Chemical structure of amylose	33
Figure 2.3: Chemical structure of amylopectin	34
Figure 2.4: Structure of starch	35
Figure 2.5: Gelatinization and retrogradation of starch	36
Figure 2.6: Diagram of an extruder	37
Figure 2.7: Diagram of the expansion process during extrusion	38
Figure 2.8: Main factors influencing expansion during extrusion	39
Figure 2.9: Sorption isotherm for the typical food product	40
Figure 2.10: Overlay of sorption isotherm and plasticizing effect of water on $T_{\rm g}$ of starch .	41
Figure 2.11: General diagram of a DSC curve	42
Figure 2.12: FTIR spectra of freeze-dried gelatinized native potato starch (PN)	43
Figure 2.13: Schematic diagram of X-ray microcomputed tomography	44
Figure 3.1: FTIR spectrum showing crystalline and amorphous starch peaks	67
Figure 3.2: Distribution of pores throughout storage	69
Figure 3.3: Pore diameter distribution during storage	71
Figure 3.4: Pore diameter distribution at different times post-cutting	73
Figure 3.5: 3-D image of distribution of high density material	74
Figure 3.6: 2-D image of distribution of high density material	75

Figure 4.1: Sorption isotherm of starch extrudate	94
Figure 4.2: MRI images of starch extrudates	96

CHAPTER 1

INTRODUCTION

As the number of extruded starch products expands in the food industry, a better understanding is needed of changes in these products occurring during storage that may lead to loss of quality. Typically, extruded starch is studied using analytical methods, such as moisture analysis, Differential Scanning Calorimetry (DSC), and Fourier Transform Infrared Spectroscopy (FTIR). However, analytical methods lack the ability to provide information about the distribution of structural changes and moisture migration in these products.

Imaging techniques have the ability to supplement analytical techniques by supplying information on the distribution of these changes. Conventional imaging methods used when studying starch extrudates are light microscopy (Altan, McCarthy & Maskan, 2009; Chaudhary, Torley, Halley, McCaffery & Chaudhary, 2009) and electron microscopy (Lopez-Rubio, Flanagan, Shrestha, Gidley & Gilbert, 2008; Mahasukhonthachat, Sopade & Gidley, 2010; Majdzadeh-Ardakani & Nazari, 2010). However, these techniques are generally used to image cross-sections or surface structures of the material and are not used to provide images of moisture in these products.

The goal of this study was to use imaging methods that are rarely used on starch extrudates to provide a more complete picture of the changes occurring during storage. The third chapter describes the use of Microcomputed tomography (microCT) during storage of starch extrudates. MicroCT is a three-dimensional imaging technique that uses a series of X-rays through a rotating object to produce an image based on differences in density within the sample.

This method is quick, non-destructive, and relatively inexpensive. It can be used to study structural changes in a sample, such as changes in the pores and density differences within a sample.

In addition to structural changes, changes in moisture can also affect the quality of these products. The fourth chapter describes the use of Magnetic Resonance Imaging (MRI) on starch extrudates during storage. MRI is an imaging technique that uses a magnetic field and a series of radio frequency pulses to produce an image. This technique can be used to produce images of the moisture in a material, and different pulse sequences can be applied to image different characteristics of the moisture. The utilization of both of these imaging methods during storage should provide a better understanding of changes in structure and moisture that can affect the quality of these products and limit their shelf-life.

References

- Altan, A., McCarthy, K. L., & Maskan, M. (2009). Effect of Extrusion Cooking on Functional Properties and in vitro Starch Digestibility of Barley-Based Extrudates from Fruit and Vegetable By-Products. *Journal of Food Science*, 74(2), E77-E86.
- Chaudhary, A. L., Torley, P. J., Halley, P. J., McCaffery, N., & Chaudhary, D. S. (2009).

 Amylose content and chemical modification effects on thermoplastic starch from maize
 Processing and characterisation using conventional polymer equipment. *Carbohydrate Polymers*, 78(4), 917-925.
- Lopez-Rubio, A., Flanagan, B. M., Shrestha, A. K., Gidley, M. J., & Gilbert, E. P. (2008).

 Molecular rearrangement of starch during in vitro digestion: Toward a better understanding of enzyme resistant starch formation in processed starches.

 Biomacromolecules, 9(7), 1951-1958.
- Mahasukhonthachat, K., Sopade, P. A., & Gidley, M. J. (2010). Kinetics of starch digestion and functional properties of twin-screw extruded sorghum. *Journal of Cereal Science*, *51*(3), 392-401.
- Majdzadeh-Ardakani, K., & Nazari, B. (2010). Improving the mechanical properties of thermoplastic starch/poly(vinyl alcohol)/clay nanocomposites. *Composites Science and Technology*, 70(10), 1557-1563.

CHAPTER 2

LITERATURE REVIEW

Extrusion of starch-based materials, such as cereals, is widely used throughout the food industry to make products such as pasta, cereal, pet food, and, particularly, snack foods. Extrusion provides a method of cooking, shaping, and expanding these products with a high degree of control and repeatability. Staling of extruded starch products, which can occur due to moisture migration and/or recrystallization of the starch molecules, can lead to moisture-rich areas, textural changes, and an overall loss of product quality. Typically, these types of products are studied using various analytical techniques, such as Fourier Transform Infrared Spectroscopy (FTIR) and Differential Scanning Calorimetry (DSC), but very few imaging techniques have been applied to these types of materials. As the snack food industry increases its production of these types of products, the methods for assessing the quality of these products should be expanded to include more imaging techniques to provide a better understanding of the deterioration of quality during storage.

Starch

Starch is the storage carbohydrate in plants, such as cereals, tubers, fruits, and beans. The starch is stored in granules that vary in size and shape based on the plant source (Fig. 2.1, Table 2.1) (Singh, Singh, Kaur, Sodhi & Gill, 2003; Tester, Karkalas & Qi, 2004). Starch granules are characterized by a birefringent maltese cross that can be viewed with polarized light microscopy.

This cross is formed from the radial arrangement of the starch molecules around its center, the hilum, from which the starch granules start to develop.

Starch consists of two types of polysaccharides arranged as repeating units of D-glucose – amylose and amylopectin. Amylose is a linear molecule made up of an average of 1000 repeating units of $\alpha(1-4)$ -linked glucose molecules with the occasional $\alpha(1-6)$ -linked branch (Fig. 2.2) (Tester et al., 2004). Amylopectin is a highly branched molecule containing up to hundreds-of-thousands repeating $\alpha(1-4)$ -linked glucose molecules with many $\alpha(1-6)$ -linked branches that can vary in length based on the botanical source (Fig. 2.3, Fig. 2.4a) (Sajilata, Singhal & Kulkarni, 2006; Tester et al., 2004). Starch from cereal grains typically consists of 20-30% amylose and 70-80% amylopectin, but these values can change based on different botanical sources.

Within the starch granule, there are crystalline and amorphous regions that are characterized by the arrangement of the amylose and amylopectin. The crystalline regions occur where the branches of the amylopectin molecules arranged around the hilum are tightly packed, while the amorphous regions are found at the branch points of the amylopectin molecules where the amylose molecules cluster together (Fig. 2.4b and 2.4c) (Sajilata et al., 2006). Amylose molecules and some branches of amylopectin molecules can easily form single and double helices, which affect the packing of these molecules within the radial arrangement around the hilum (Fig. 2.4d).

The functional properties of starch vary based on the botanical source due to the different amounts of amylose and amylopectin as well as the difference in the branch lengths and degree of polymerization of these molecules. In addition, small amounts of lipids, phosphates, and proteins can be found within starch granules that interact with the starch molecules. Lipids can

form a complex with amylose and phosphates can bond to amylopectin, while proteins can interact with oxidized molecules of both, which can also affect the functional properties of the starch (Abd Karim, Norziah & Seow, 2000; Singh, Gamlath & Wakeling, 2007b).

Starch is useful as a thickening agent because it undergoes an irreversible process, called gelatinization, when exposed to heat and water (Fig. 2.5). When enough heat is applied to starch granules in water, hydrophobic interactions and hydrogen bonds are broken disrupting the semicrystalline structure and allowing some of the water to enter the granules and some of the amylose molecules to leave the granules and form junctions with each other increasing the viscosity (Jane, 2007). At this gelatinization temperature, the granules are now characterized by swelling, melting of the native semicrystalline structure, loss of the birefringent maltese cross, and solubilization of starch (Sullivan & Johnson, 1964). Solubilization of starch makes it much easier to digest, making it an important process in preparing starch for consumption in food products. Addition of further heat leads to pasting, in which there is increased swelling and viscosity, higher loss of amylose, and total disruption of the granule.

Many different factors can affect gelatinization, including the temperature used, the amount of moisture, the amount of time in the presence of heat and water, and the stirring or mixing of the starch-water slurry (Sajilata et al., 2006; Singh et al., 2003; Tester et al., 2004). In addition, the presence of additives, such as acids, sugars, fats, proteins, or salts, will affect gelatinization of the starch. One of the main factors affecting the gelatinization is the type of material used. The type of material can vary based on the size, the source, and the amount of amylose and amylopectin (Tester et al., 2004). High amylose starches (52-80% amylose content) have a higher gelatinization temperature than native starches because the terminal branches on the amylopectin molecules are longer, so more heat is needed to break down the structure. High

amylopectin starches (>99% amylopectin), or waxy starches, lead to higher gelatinization temperatures than native starches because of the larger amount of crystallinity (Sajilata et al., 2006; Singh et al., 2003; Tester et al., 2004). The gelatinization temperature is reported as a range specific to different types of starch because of differences in amylose content and amylopectin structure within a given starch population.

Retrogradation, an important process involved in staling of starch products, occurs when gelatinized starch cools and sits over time (Fig. 2.5) (Tester et al., 2004). Some of the starch molecules start to recrystallize, which leads to moisture-rich areas or syneresis (weeping of water) when the crystallized molecules constrict the junctions within the gel. Amylose molecules retrograde in a matter of hours or days, while amylopectin molecules take much longer to retrograde. Although amylose molecules retrograde much faster than amylopectin molecules, amylopectin retrogradation is the main cause of staling in these starch products due to the long-term changes occurring during recrystallization of amylopectin. Amylopectin molecules that have longer chains tend to undergo more retrogradation (Wang, Wang & Porter, 2002). This process can be accelerated by storing the starch product at 4°C (Patel & Seetharaman, 2010).

Starch has many different functional properties depending on the type and degree of modification. Native starch is most useful as a thickening agent, but other functional properties can be obtained via modification. Modifications include acid hydrolysis, cross-linking, and substitution of other molecules for the hydroxyl groups on the C2, C3, and C6 positions of the glucose molecules within the starch backbone (Jane, 2007; Singh, Kaur & McCarthy, 2007a; Whistler, 1964). Both the type and degree of substitution affect the functional properties as well. For instance, substitution with octenyl succinate makes starch a good emulsifier. A higher degree of substitution leads to a greater emulsifying capacity. Certain starches are also known as

resistant starches because they are resistant to digestion due to physical barriers (Type I), high amylose content (Type II), retrogradation (Type III), or chemical modification (Type IV) (Sajilata et al., 2006). Functional properties of these starches vary widely, including as functional dietary fiber, texture modifiers, and gelling agents, because of the vast array of modifications and types of resistant starches. In addition, some modifications are designed to increase freeze-thaw stability, expansion, and stability to processing, making these modified starches very useful in extruded starch products.

Extrusion

Extrusion is a forming process that is widely used throughout the food industry, especially in the snack food industry. Cold extrusion can be used to mix and form products, such as pasta, but most extruded products use a high-temperature, short-time process to cook and expand the product while forming (Fellows, 2009). Extrusion uses a combination of pressure, moisture, shear, and heat to produce the desired food product. This process uses relatively dry materials in combination with low moisture to gelatinize starch, denature enzymes, polymerize proteins, plasticize food, reduce microbial load, retain natural colors and flavors of foods, and form the product into the desired form (Bhandari, D'Arcy & Young, 2001; Fellows, 2000; Qu & Wang, 1994; Singh et al., 2007a). This process has the advantages of low cost, high repeatability, high productivity, versatility, energy efficiency, and no effluents for waste (Fellows, 2009).

Extruders have a fairly simple design to perform this complex process (Fig. 2.6) (Fellows, 2009). Extruders consist of a hopper that introduces water and other materials to the screws inside the barrel of the extruder. Extruders can have a single screw or twin screw design, and the twin screw design can have co-rotating or counter-rotating screws. As the extruder runs,

turn, they generate heat and shear forces as the mixing material moves towards the die, a hole or slit at the end of the extruder that can be the shape and size needed to produce the desired product. The addition of mixing paddles to the screws increases the shear forces and the amount of mixing. In addition, the temperature can be monitored and controlled to maintain the desired temperature using periodic thermocouples along the barrel. As the material approaches the die, the pressure, temperature, and shear increase due to compression. Then, when the material is forced through the die, the resulting temperature and pressure drop causes the water to convert to steam. Expansion occurs within the product if the resulting drop in temperature and pressure is high enough to cause nucleation sites for flash boiling of the water (Fig. 2.7) (Moraru & Kokini, 2003). In addition, the rapid cooling of the material directly exposed to the cooler temperature can lead to case hardening of the outside of the extruded product. Many factors can affect the extrusion process as shown in Fig. 2.8 (Stevens & Covas, 1995).

When starch undergoes extrusion in the presence of a sufficient amount of water and a high enough temperature, gelatinization occurs. The amylose molecules contribute to gel formation, while the amylopectin molecules contribute to the viscosity of the product (Singh et al., 2007a). However, amylose and amylopectin molecules do not go unscathed. The high shear forces produced during extrusion break down these starch components into lower molecular weight molecules by shearing some of the glycosidic bonds between glucose molecules. Amylopectin is much more susceptible to these shear forces due to its highly branched nature (Politz, Timpa & Wasserman, 1994). Since the amount of shear can be controlled by the screw design, the screw configuration can be tailored to provide the desired amount of starch breakdown from very little degradation to degradation into dextrins or single glucose molecules

(Gautam & Choudhury, 1999). Another reaction that occurs during extrusion of starch is the formation of lipid-amylose complexes. This reaction can be controlled by selection of the starch source to get the desired amylose content and the amount and type of lipids added to the mixture or present in the original starch. In addition, this reaction may be increased by higher viscosity and longer residence time in the extruder (Singh & Smith, 1997).

Analytical Techniques

Analytical techniques are very useful when studying extruded starch products. These methods provide useful information about the material, including quality changes that occur during storage. Some of the most widely used techniques for studying extruded starch products and the information they can provide are described here. However, all of these techniques lack the ability to provide a visual representation of structural changes that occur and the distribution of these changes during storage throughout the material.

Analysis of water

Moisture analysis is essential to the study of extruded starch products. The moisture in a system can have a profound effect on the quality of the product and the speed of the staling process (Bourlieu, Guillard, Powell, Valles-Pamies, Guilbert & Gontard, 2008; Kester & Fennema, 1986; Lim & Jane, 1994; Roca, Guillard, Guilbert & Gontard, 2006). Typically, extruded starch products are low moisture products that maintain a crispy texture without any sogginess, but moisture migration can affect texture changes through plasticization of starch. In addition, the rate of retrogradation during staling depends highly on the moisture content (Abd Karim et al., 2000; BeMiller & Whistler, 2009). Retrogradation occurs when the solids content

of the starch product is between 10 - 80%, but not at very high or very low moisture contents (Longton & Legrys, 1981; Marsh & Blanshard, 1988; Zeleznak & Hoseney, 1986). Retrogradation occurs faster when the material is stored at a temperature higher than the glass transition temperature (T_g), the temperature at which the material transitions from glassy to rubbery, as this provides an environment that promotes the nucleation and growth of the crystallites (Jouppila & Roos, 1997). If the moisture content during storage is higher than 50%, retrogradation rate decreases, which is probably due to dilution of the starch components within the sample (BeMiller et al., 2009). Analysis of moisture content helps to produce consistent product and to control changes during storage, but this method does not provide the complete picture of moisture activity.

In addition to the importance of the moisture content, maintenance of the water activity (a_w) in the sample is critical for controlling the texture of the product and the rate of staling. Most microbial growth occurs at high water activities and the rate of retrogradation decreases at lower water activities due to the lower moisture content (Abd Karim et al., 2000). While moisture content provides information about the total amount of water, both free and bound, in the sample, water activity is more of a measure of the available water in the system. It is defined as the ratio of vapor pressure of water in the sample to vapor pressure of pure water and can be determined using a water activity balance (Hui, 2007). Water activity provides useful information about the mechanisms that can occur during staling based on the availability of the water in the material, but it still does not provide insight into the distribution of these changes or moisture migration because it is performed on bulk samples.

Another way to observe the behavior of the water in the sample is to combine the moisture content and the water activity by generating a sorption isotherm. The sorption isotherm

can be generated by removing all of the moisture from the sample (for adsorption isotherm) or increasing the moisture in the sample to a water activity of ~1.0 (for desorption isotherm) and then allowing the sample to equilibrate to different environments of varying water activities (or relative humidities) at a constant temperature. The plot of the moisture contents at the various water activities shows the sorption isotherm (Fig. 2.9) (Andrade, Lemus & Perez, 2011). There are five general curve shapes that have been found for sorption isotherms, but most food products are the sigmoidal-shaped type 2, as seen in Fig. 2.9. Within this sigmoidal-shaped isotherm, there are three areas: A) the monolayer area, B) the multilayer area, and C) the liquid or free water area. The monolayer area, seen at low water activities, is observed as water molecules start to bind to the surface of the food product, forming a monolayer. Once the monolayer has been formed, additional water attaches to the monolayer, forming a multilayer. As additional water is introduced to the sample, it is no longer bound to the surface or the monolayer and becomes known as free water that can move throughout the sample.

The sorption isotherm is useful in predicting the best storage conditions for a product to prevent staling based on water behavior in the product at different storage conditions. A plot of the T_g overlaying the sorption isotherm can provide even more information on the storage conditions necessary to prevent or reduce retrogradation (Fig. 2.10) (Jouppila et al., 1997). As mentioned previously, the product becomes unstable at temperature higher than the T_g , promoting nucleation and growth of the crystals. Therefore, at higher water activities where the T_g decreases, storage at ambient or refrigeration temperatures promotes retrogradation. This graph can help determine the activity of both the water and the starch at various storage temperatures, but it does not provide information on the distribution of these changes within the product.

Differential Scanning Calorimetry (DSC)

DSC is a quick, but somewhat expensive, method for analyzing the thermal properties of different products that can be used with a wide range of moisture contents and requires only a small amount of sample (5-10 mg) (Nakazawa, Noguchi, Takahashi & Takada, 1985). It works by comparing the heat flow changes during programmed heating or cooling between a sealed pan containing a sample of the product to an sealed reference pan, which is typically empty. Because the temperature and the rate of temperature change are strictly controlled by the user-defined program, the difference in heat flow between the sample and the reference pans changes based on the amount of heat energy used or lost when the sample undergoes a transition. During an endothermic transition, such as starch gelatinization, the amount of heat flow used will increase for the sample because the heat provides the energy for the melting of the crystallites, which will be displayed as a peak when plotting the heat flow against the temperature (Fig. 2.11).

The shape, size, and location of these peaks can provide information about the thermal transition that occurs, such as the temperature range of the transition, the amount of energy needed per gram to affect the transition, and the miscibility of the ingredients based on the presence or absence of overlapping peaks. The direction of the peak will indicate whether the reaction is endothermic or exothermic, and the area under the peak is a measure of the enthalpic change (ΔH) during the transition. For starch products, the gelatinization peak can also be affected by the type of starch used, the amount and type of processing, the presence of additional ingredients, and the amount of water in the sample. Gelatinization peaks tend to occur around 80°C, so starch granules that are ungelatinized during processing provide an endothermic peak near this temperature (Lamberts, Gomand, Derycke & Delcour, 2009). The size and shape of the peak can indicate the amount of ungelatinized starch still remaining in the product.

During the staling process, a peak is observed for retrograded amylose between 120 and 170°C, while a peak for retrograded amylopectin is observed between 40 and 100°C (Eerlingen, Jacobs & Delcour, 1994; Sievert & Pomeranz, 1989). Recrystallized amylose is more stable than recrystallized amylopectin, so more heat is needed to melt the crystallites giving it a higher transition temperature. These peaks observed for recrystallized amylose and amylopectin can be highly affected by the storage conditions with storage temperature and moisture content affecting the rate of retrogradation and the stability of the retrograded starch (Eliasson, 1985; Jang & Pyun, 1997; Jankowski & Rha, 1986; Nakazawa et al., 1985). Because this technique is typically performed using a small sample size of 5-10 mg, small areas of retrogradation can be missed if retrogradation is not uniform throughout the product. In addition, with such a small sample size, it is difficult to determine the distribution of the retrogradation without extensive and selective sampling.

Fourier Transform Infrared Spectroscopy (FTIR)

FTIR is a quick, non-destructive method that provides both qualitative and quantitative data about the sample being tested. Infrared (IR) radiation in the mid-IR range (4000-400 cm⁻¹) is reflected, absorbed, or transmitted through the sample. The spectrum produced when plotting the intensity against the wavelength provides information about the different bonds in the sample based on absorbance of the radiation, with each sample producing a unique spectrum. The wavelength of the absorbance peak corresponds to the frequency of the vibrations between the bonds in the sample, so the location of the peak provides information about the types of bonds in the sample. The size of the absorbance peak corresponds to the amount of material present.

FTIR can be very useful when studying retrogradation of starch during the staling process. As the structure of the starch becomes more ordered during retrogradation, band narrowing occurs in the 1300-800 cm⁻¹ range of the spectrum (Abd Karim et al., 2000; Wilson, Goodfellow, Belton, Osborne, Oliver & Russell, 1991). In addition, characteristic peaks can be seen for the ordered, crystalline starch (~1047 cm⁻¹) and the amorphous starch (~1022 cm⁻¹) (Fig. 2.12) (Abd Karim et al., 2000; Smits, Ruhnau, Vliegenthart & van Soest, 1998). As retrogradation progresses during storage, the ratio of the crystalline to amorphous peak shifts towards one as the crystalline area increases and the amorphous area decreases. Also, as previously mentioned, retrogradation is observed to occur much more rapidly when the starch is stored at high relative humidity (90% RH) as compared to lower relative humidity (30% RH) (Smits et al., 1998). This method can provide information on retrogradation at a larger scale than DSC, but does not provide information on the distribution of the changes occurring due to retrogradation.

Imaging Techniques

Imaging methods are not widely used on extruded starch products. Typical imaging studies of these types of materials include light microscopy (Chaudhary, Torley, Halley, McCaffery & Chaudhary, 2009; Enrione, Hill & Mitchell, 2007; Salmenkallio-Marttila, Heinio, Myllymaki, Lille, Autio & Poutanen, 2004), polarized light microscopy (Altan, McCarthy & Maskan, 2009; Bhatnagar & Hanna, 1996; Mousia, Farhat, Pearson, Chesters & Mitchell, 2001), and electron microscopy (Batterman-Azcona, Lawton & Hamaker, 1999; Dean, Do, Petinakis & Yu, 2008; Lopez-Rubio, Flanagan, Shrestha, Gidley & Gilbert, 2008; Lopez-Rubio, Htoon & Gilbert, 2007; Ma, Yu & Ma, 2005; Mahasukhonthachat, Sopade & Gidley, 2010; Majdzadeh-

Ardakani & Nazari, 2010; Simmons & Thomas, 1995; Ushakumari, Latha & Malleshi, 2004; Zhuang et al., 2010). These methods have demonstrated their usefulness, but each of them has their own set of limitations.

Light microscopy is a quick and inexpensive method that determines the basic layout of a cross-section of the material, the distribution of the pores, the general shape of different crystalline structures, and the thickness of any case hardening that occurred during the extrusion process. However, the resolution is limited to a maximum of 100 - 500 nm and staining is usually required. Polarized light microscopy can show the location of ungelatinized starch granules throughout the cross-section because the birefringent maltese cross in intact starch granules is visible with polarized light (Hui, 2007). However, only certain structures can be seen and resolution is limited. Both Scanning electron microscopy (SEM) and Transmission electron microscopy (TEM) provide excellent resolution up to 0.2 - 0.5 nm, but both are expensive methods that require time-consuming and intricate preparation methods. In addition, SEM is limited to surface structures, while TEM is limited to cross-sections of the material with a very limited field of view.

All of these methods destroy the sample through the fixation process or through sectioning, preventing it from being studied by other methods in addition to microscopy, and these methods lack the ability to show internal structures in a three-dimensional format with the exceptions of the difficult tasks of serial sectioning and reconstruction using multiple TEM micrographs of neighboring sections or focused ion-beam reconstruction combined with SEM. In addition, none of these imaging methods observes the moisture in the material. New imaging methods can be applied to overcome these limitations and provide a more complete picture of the structure of these materials.

Micro Computed Tomography (MicroCT)

MicroCT is an imaging technique that uses a series of X-rays to generate a 3-D image of an intact bulk sample. This method works by placing a sample on a rotating platform and a series of 2-D X-rays images are taken as the sample is rotated (Fig. 2.13) (Lim & Barigou, 2004). The X-rays are differentially absorbed by the material based on differences in density within the materials, with higher density areas absorbing more X-rays. A series of algorithms are used to construct a 3-D image of the sample by combining the array of 2-D X-ray images into one image. Areas of different densities, such as pores and solids of different densities, should be resolved provided that the difference in densities is detectable.

MicroCT image acquisition is a quick, non-destructive method that requires no sample preparation. In addition, it is relatively inexpensive compared to electron microscopy. The resolution achieved with this method varies based on the size of the material and can be optimized based on the signal generated by the density differences in the material and the size of the structures within the material. The application of microCT can provide very useful structural information in a 3-D format with relative ease without destruction of the sample, which could be extremely useful in the study of foods (Babin, Della Valle, Dendievel, Lourdin & Salvo, 2007; Lim et al., 2004; van Dalen, Blonk, van Aalst & Hendriks, 2003).

MicroCT has not been widely used in the study of food and has only started to make a more widespread appearance in the literature since 2007. Most of these studies have focused on using this technique to characterize the porosity under different treatment conditions in a wide range of food items, such as ice cream (Pinzer, Medebach, Limbach, Dubois, Stampanoni & Schneebeli, 2012), fried chicken nuggets (Adedeji & Ngadi, 2009; Adedeji & Ngadi, 2011), baked goods (Esveld, van der Sman, van Dalen, van Duynhoven & Meinders, 2012; Lim et al.,

2004), and cereals/grains (Chaunier, Della Valle & Lourdin, 2007; Guessasma, Chaunier, Della Valle & Lourdin, 2011; van Dalen et al., 2003), but only a few studies have focused on extruded starch (Babin et al., 2007; Plews, Atkinson & McGrane, 2009).

While some previous work using microCT has been done on starch extrudates, none of these studies has involved changes observed during storage. Babin et al. (2007) focused on the basic cellular structure of maize starch extrudates of different amylose contents (0-70%). The mean cell size and cell wall thickness varied based on the amylose content and the extrusion conditions used were from 0.2-5 mm and 75-630 μ m, respectively. Products of similar densities were compared based on their capacity to rupture and those with smaller cell size (< 2 mm diameter) and cell wall thickness (< 300 μ m) were more resistant to rupture. This study showed the usefulness of microCT in studying these types of materials, but did not use the capabilities of microCT to its full potential to look at different structures within the solid material or to characterize the pore networks within the extrudates.

Plews et al. (2009) used microCT to study starch-based extrudates. This study focused on the ability of microCT to characterize the differences in the pore networks between low- and high-expansion extrudates. The study combined microCT with density results to show that microCT analysis of the overall porosity in a product is comparable to traditional methods for determining the volume of the pores. This study also visualized the different pore sizes and shapes, the distribution of the pores, and the connections between pores. High density areas observed in the solid material were assumed to be protein with little justification. Although this study focused on pore characterization in these extrudates, it did not focus on differences within the solid material even though some differences were noted in the study.

These previous studies demonstrate the efficacy of using microCT to image starch extrudates. In addition, microCT is considered the most promising technique for characterizing structure in food engineering (van Dalen et al., 2003). Because the microstructure of a material affects the texture properties, the use of microCT to study the microstructure should provide structural information that can provide insight into texture changes. More information on microstructure changes during storage could provide insight into texture changes and quality loss.

Magnetic Resonance Imaging (MRI)

MRI is a useful technique that works by placing the sample within a magnetic field to align the magnetization of the atoms in the sample parallel to the magnetic field. Radio frequency fields are applied to alter the magnetization alignment of the frequency-specific nuclei in the desired fashion. As the radio frequency field is removed, the magnetization realigns to the magnetic field and produces a detectable signal. This signal can be transformed into an image based on the nucleus density distribution throughout the imaged area of the sample. Different protocols can be applied to the process to produce different types of images and can be applied using different frequencies to select the desired type of nuclei. The nuclei that are being used to form the image must be in high abundance and have non-zero nuclear spin, with each unpaired neutron and proton providing a spin of ½ (Table 2.2). This method allows for the visualization of the desired nuclei within a material in a quick, non-destructive manner at a relatively low cost, but requires expertise for optimizing the process and analyzing the resultant data.

MRI has become more widely used in the study of food in recent years. Some previous studies have focused on moisture changes during tempering of rice kernels (Hwang, Cheng,

Chang, Lur & Lin, 2009), moisture distributions in blueberries (Gamble, 1994), grains (Himmelsbach & Gamble, 1997), whey protein gels (Oztop, Rosenberg, Rosenberg, McCarthy & McCarthy, 2010), soy protein extrudates (Chen, Wei & Zhang, 2010), and food colloids (Cornillon & Salim, 2000; Mariette, 2009). Changes in moisture in starch extrudates have not been previously studied using MRI. However, Ruan et al. (1996) studied changes in the moisture distribution and water mobility in sweet rolls, a starch-based product, stored at room temperature over five days using spin-echo and T2 MRI techniques. This study found a shift in the moisture from the crumb to the crust during storage. However, the mobility of the water increased in the center of the rolls and decreased in the crust during storage, which does not follow the pattern displayed by the moisture distribution. These differences were hypothesized to be the result of physicochemical processes taking place during storage and were supported by DSC results indicating that starch retrogradation occurred during the five days of storage, which would have affected the matrix containing the moisture. This study illustrated that changes observed in the mobility of the water were not simply reflective of changes in the moisture content, but that a much more complex relationship was evident due to the nature of the starch-based matrix containing the moisture that would not have been observed using traditional analytical or imaging techniques.

Conclusions

Analytical methods used to study extruded starch products provide useful information but not the complete picture. These methods lack the ability to provide information about the distribution of structural changes and moisture migration that occur in these types of products. Imaging methods can help to complete the picture by providing visual images of the changes

occurring during storage. However, the imaging methods that are typically used to study these products are limited in their ability to visualize the distribution of structural changes and moisture migration.

Novel imaging methods, such as microCT and MRI, can help to fill in the gaps in knowledge. MicroCT can be used to study changes in the microstructure of extrudates, which provide the backbone for changes in texture observed during storage. MRI can be used to study changes in the distribution of moisture during storage, which can negatively affect the texture. Application of these imaging methods during storage should provide a clearer idea of changes that lead to quality loss in these products.

References

- Abd Karim, A., Norziah, M. H., & Seow, C. C. (2000). Methods for the study of starch retrogradation. *Food Chemistry*, 71(1), 9-36.
- Adedeji, A. A., & Ngadi, M. O. (2009). 3-D Imaging of Deep-Fat Fried Chicken Nuggets

 Breading Coating Using X-Ray Micro-CT. *International Journal of Food Engineering*,

 5(4).
- Adedeji, A. A., & Ngadi, M. O. (2011). Microstructural characterization of deep-fat fried breaded chicken nuggets using x-ray micro-computed tomography. *Journal of Food Process Engineering*, 34(6), 2205-2219.
- Altan, A., McCarthy, K. L., & Maskan, M. (2009). Effect of Extrusion Cooking on Functional Properties and in vitro Starch Digestibility of Barley-Based Extrudates from Fruit and Vegetable By-Products. *Journal of Food Science*, 74(2), E77-E86.
- Anasys (2012). DTA and DSC webpage, www.anasys.co.uk/library/dsc2.htm.
- Andrade, R. D., Lemus, R., & Perez, C. E. (2011). Models of sorption istherms for food: Uses and limitations. *Vitae-Revista De La Facultad De Quimica Farmaceutica*, 18(3), 324-333.
- Babin, P., Della Valle, G., Dendievel, R., Lourdin, D., & Salvo, L. (2007). X-ray tomography study of the cellular structure of extruded starches and its relations with expansion phenomenon and foam mechanical properties. *Carbohydrate Polymers*, 68(2), 329-340.
- Batterman-Azcona, S. J., Lawton, J. W., & Hamaker, B. R. (1999). Effect of specific mechanical energy on protein bodies and alpha-zeins in corn flour extrudates. *Cereal Chemistry*, 76(2), 316-320.

- BeMiller, J. N., & Whistler, R. L., eds (2009). *Starch: Chemistry and Technology*. Burlington, MA: Elsevier.
- Bhandari, B., D'Arcy, B., & Young, G. (2001). Flavour retention during high temperature short time extrusion cooking process: a review. *International Journal of Food Science and Technology*, 36(5), 453-461.
- Bhatnagar, S., & Hanna, M. A. (1996). Starch-stearic acid complex development within single and twin screw extruders. *Journal of Food Science*, 61(4), 778-782.
- Bourlieu, C., Guillard, V., Powell, H., Valles-Pamies, B., Guilbert, S., & Gontard, N. (2008).

 Modelling and control of moisture transfers in high, intermediate and low a(w) composite food. *Food Chemistry*, 106(4), 1350-1358.
- Chaudhary, A. L., Torley, P. J., Halley, P. J., McCaffery, N., & Chaudhary, D. S. (2009).
 Amylose content and chemical modification effects on thermoplastic starch from maize Processing and characterisation using conventional polymer equipment. *Carbohydrate Polymers*, 78(4), 917-925.
- Chaunier, L., Della Valle, G., & Lourdin, D. (2007). Relationships between texture, mechanical properties and structure of cornflakes. *Food Research International*, 40(4), 493-503.
- Chen, F. L., Wei, Y. M., & Zhang, B. (2010). Characterization of water state and distribution in textured soybean protein using DSC and NMR. *Journal of Food Engineering*, 100(3), 522-526.
- Cornillon, P., & Salim, L. C. (2000). Characterization of water mobility and distribution in lowand intermediate-moisture food systems. *Magnetic Resonance Imaging*, 18(3), 335-341.

- Dean, K. M., Do, M. D., Petinakis, E., & Yu, L. (2008). Key interactions in biodegradable thermoplastic starch/poly(vinyl alcohol)/montmorillonite micro- and nanocomposites. *Composites Science and Technology*, 68(6), 1453-1462.
- Eerlingen, R. C., Jacobs, H., & Delcour, J. A. (1994). Enzyme-resistant starch. 5. Effect of retrogradation of waxy maize starch on enzyme susceptibility. *Cereal Chemistry*, 71(4), 351-355.
- Eliasson, A. C. (1985). Starch-lipid interactions studied by differential scanning calorimetry. *Thermochimica Acta*, 95(2), 369-374.
- Enrione, J. I., Hill, S. E., & Mitchell, J. R. (2007). Sorption and diffusional studies of extruded waxy maize starch-glycerol systems. *Starch-Starke*, *59*(1), 1-9.
- Esveld, D. C., van der Sman, R. G. M., van Dalen, G., van Duynhoven, J. P. M., & Meinders, M. B. J. (2012). Effect of morphology on water sorption in cellular solid foods. Part I: Pore scale network model. *Journal of Food Engineering*, 109(2), 301-310.
- Fellows, P. (2000). Food Processing Technology: Principles and Practice. Cambridge: Woodhead Publishing Ltd.
- Fellows, P. J. (2009). Food Processing Technology: Principles and Practice. Boca Raton, FL: CRC Press.
- Gamble, G. R. (1994). Noninvasive determination of freezing effects in blueberry fruit tissue by magnetic-resonance-imaging. *Journal of Food Science*, *59*(3), 571-573.
- Gautam, A., & Choudhury, G. S. (1999). Screw configuration effects on starch breakdown during twin-screw extrusion of rice flour. *Journal of Food Processing and Preservation*, 23(5), 355-375.

- Guessasma, S., Chaunier, L., Della Valle, G., & Lourdin, D. (2011). Mechanical modelling of cereal solid foods. *Trends in Food Science & Technology*, 22(4), 142-153.
- Himmelsbach, D. S., & Gamble, G. R. (1997). NMR, FT-IR, and FT-Raman spectroscopic imaging of grains. In: *International Workshop on Application of Magnetic Resonance and Other Spectroscopic Techniques to Food Science*.
- Hornak, J. P. (1997-9). The Basics of NMR. Rochester, NY: Rochester Institute of Technology.
- Hui, Y. H., ed (2007). Food Chemistry: Principles and Applications. Sacramento, CA: Science Technology System.
- Hwang, S. S., Cheng, Y. C., Chang, C., Lur, H. S., & Lin, T. T. (2009). Magnetic resonance imaging and analyses of tempering processes in rice kernels. *Journal of Cereal Science*, 50(1), 36-42.
- Jane, J. L. (2007). Carbohydrates: Basic Concepts. In: Y. H. Hui, *Food Chemistry: Principles* and Applications. West Sacramento, CA: Science Technology System.
- Jang, J. K., & Pyun, Y. R. (1997). Effect of moisture level on the crystallinity of wheat starch aged at different temperatures. *Starch-Starke*, 49(7-8), 272-277.
- Jankowski, T., & Rha, C. K. (1986). Differential scanning calorimetry study of the wheat-grain cooking process. *Starch-Starke*, *38*(2), 45-48.
- Jouppila, K., & Roos, Y. H. (1997). The physical state of amorphous corn starch and its impact on crystallization. *Carbohydrate Polymers*, 32(2), 95-104.
- Kester, J. J., & Fennema, O. R. (1986). Edible films and coatings A review. *Food Technology*, 40(12), 47-59.

- Lamberts, L., Gomand, S. V., Derycke, V., & Delcour, J. A. (2009). Presence of Amylose Crystallites in Parboiled Rice. *Journal of Agricultural and Food Chemistry*, *57*(8), 3210-3216.
- Lim, K. S., & Barigou, M. (2004). X-ray micro-computed tomography of cellular food products. Food Research International, 37(10), 1001-1012.
- Lim, S., & Jane, J. (1994). Storage stability of injection-molded starch-zein plastics under dry and humid conditions. *Journal of Polymers and the Environment*, 2(2), 111.
- Longton, J., & Legrys, G. A. (1981). Differential scanning calorimetry studies on the crystallinity of aging wheat-starch gels. *Starke*, *33*(12), 410-414.
- Lopez-Rubio, A., Flanagan, B. M., Shrestha, A. K., Gidley, M. J., & Gilbert, E. P. (2008).

 Molecular rearrangement of starch during in vitro digestion: Toward a better understanding of enzyme resistant starch formation in processed starches.

 Biomacromolecules, 9(7), 1951-1958.
- Lopez-Rubio, A., Htoon, A., & Gilbert, E. P. (2007). Influence of extrusion and digestion on the nanostructure of high-amylose maize starch. *Biomacromolecules*, 8(5), 1564-1572.
- Ma, X. F., Yu, J. G., & Ma, Y. B. (2005). Urea and formamide as a mixed plasticizer for thermoplastic wheat flour. *Carbohydrate Polymers*, 60(1), 111-116.
- Mahasukhonthachat, K., Sopade, P. A., & Gidley, M. J. (2010). Kinetics of starch digestion and functional properties of twin-screw extruded sorghum. *Journal of Cereal Science*, 51(3), 392-401.
- Majdzadeh-Ardakani, K., & Nazari, B. (2010). Improving the mechanical properties of thermoplastic starch/poly(vinyl alcohol)/clay nanocomposites. *Composites Science and Technology*, 70(10), 1557-1563.

- Mariette, F. (2009). Investigations of food colloids by NMR and MRI. *Current Opinion in Colloid & Interface Science*, 14(3), 203-211.
- Marsh, R. D. L., & Blanshard, J. M. V. (1988). The application of polymer crystal-growth theory to the kinetics of formation of the B-amylose polymorph in a 50-percent wheat-starch gel. *Carbohydrate Polymers*, 9(4), 301-317.
- Moraru, C. I., & Kokini, J. L. (2003). Nucleation and Expansion During Extrusion and Microwave Heating of Cereal Foods. *Comprehensive Reviews in Food Science and Food Safety*, 2(4), 147-165.
- Mousia, Z., Farhat, I. A., Pearson, M., Chesters, M. A., & Mitchell, J. R. (2001). FTIR microspectroscopy study of composition fluctuations in extruded amylopectin-gelatin blends. *Biopolymers*, 62(4), 208-218.
- Nakazawa, F., Noguchi, S., Takahashi, J., & Takada, M. (1985). Retrogradation of gelatinized potato starch studied by differential scanning calorimetry. *Agricultural and Biological Chemistry*, 49(4), 953-957.
- Oztop, M. H., Rosenberg, M., Rosenberg, Y., McCarthy, K. L., & McCarthy, M. J. (2010).

 Magnetic Resonance Imaging (MRI) and Relaxation Spectrum Analysis as Methods to

 Investigate Swelling in Whey Protein Gels. *Journal of Food Science*, 75(8), E508-E515.
- Patel, B. K., & Seetharaman, K. (2010). Effect of heating rate at different moisture contents on starch retrogradation and starch-water interactions during gelatinization. *Starch-Starke*, 62(10), 538-546.
- Pinzer, B. R., Medebach, A., Limbach, H. J., Dubois, C., Stampanoni, M., & Schneebeli, M. (2012). 3D-characterization of three-phase systems using X-ray tomography: tracking the microstructural evolution in ice cream. *Soft Matter*, 8(17), 4584-4594.

- Plews, A. G., Atkinson, A., & McGrane, S. (2009). Discriminating Structural Characteristics of Starch Extrudates through X-ray Micro-tomography using a 3-D Watershed Algorithm.

 International Journal of Food Engineering, 5(1).
- Politz, M. L., Timpa, J. D., & Wasserman, B. P. (1994). Quantitative measurement of extrusion-induced starch fragmentation products in maize flour using nonaqueous automated gel-permeation chromatography. *Cereal Chemistry*, 71(6), 532-536.
- Qu, D., & Wang, S. S. (1994). Kinetics of the formations of gelatinized and melted starch at extrusion-cooking conditions. *Starch-Starke*, 46(6), 225-229.
- Roca, E., Guillard, V., Guilbert, S., & Gontard, N. (2006). Moisture migration in a cereal composite food at high water activity: Effects of initial porosity and fat content. *Journal of Cereal Science*, 43(2), 144-151.
- Ruan, R., Almaer, S., Huang, V. T., Perkins, P., Chen, P., & Fulcher, R. G. (1996). Relationship between firming and water mobility in starch-based food systems during storage. *Cereal Chemistry*, 73(3), 328-332.
- Sajilata, M. G., Singhal, R. S., & Kulkarni, P. R. (2006). Resistant starch A review.

 Comprehensive Reviews in Food Science and Food Safety, 5(1), 1-17.
- Salmenkallio-Marttila, M., Heinio, R. L., Myllymaki, O., Lille, M., Autio, K., & Poutanen, K. (2004). Relating microstructure, sensory and instrumental texture of processed oat. Agricultural and Food Science, 13(1-2), 124-137.
- Sievert, D., & Pomeranz, Y. (1989). Enzyme-resistant starch. 1. Chracterization and evaluation by enzymatic, thermoanalytical, and microscopic methods. *Cereal Chemistry*, 66(4), 342-347.

- Simmons, S., & Thomas, E. L. (1995). Structural characteristics of biodegradable thermoplastic starch/poly(ethylene-vinyl alcohol) blends. *Journal of Applied Polymer Science*, *58*(12), 2259-2285.
- Singh, J., Kaur, L., & McCarthy, O. J. (2007a). Factors influencing the physico-chemical, morphological, thermal and rheological properties of some chemically modified starches for food applications A review. *Food Hydrocolloids*, 21(1), 1-22.
- Singh, N., Singh, J., Kaur, L., Sodhi, N. S., & Gill, B. S. (2003). Morphological, thermal and rheological properties of starches from different botanical sources. *Food Chemistry*, 81(2), 219-231.
- Singh, N., & Smith, A. C. (1997). A comparison of wheat starch, whole wheat meal and oat flour in the extrusion cooking process. *Journal of Food Engineering*, *34*(1), 15-32.
- Singh, S., Gamlath, S., & Wakeling, L. (2007b). Nutritional aspects of food extrusion: a review.

 International Journal of Food Science and Technology, 42(8), 916-929.
- Smits, A. L. M., Ruhnau, F. C., Vliegenthart, J. F. G., & van Soest, J. J. G. (1998). Ageing of starch based systems as observed with FT-IR and solid state NMR spectroscopy. *Starch-Starke*, *50*(11-12), 478-483.
- Stevens, M. J., & Covas, J. A. (1995). Practical Extrusion Processes and their Applications. In:M. J. Stevens, & J. A. Covas, *Extruder Principles and Operations* (pp. 4-26): Chapman & Hall.
- Sullivan, J. W., & Johnson, J. A. (1964). Measurement of starch gelatinization by enzyme susceptibility. *Cereal Chemistry*, 41(2), 73-79.
- Tester, R. F., Karkalas, J., & Qi, X. (2004). Starch composition, fine structure and architecture. *Journal of Cereal Science*, 39(2), 151-165.

- Ushakumari, S. R., Latha, S., & Malleshi, N. G. (2004). The functional properties of popped, flaked, extruded and roller-dried foxtail millet (Setaria italica). *International Journal of Food Science and Technology*, 39(9), 907-915.
- van Dalen, G., Blonk, H., van Aalst, H., & Hendriks, C. L. (2003). 3-D imaging of foods using x-ray microtomography. G. I. T. Imaging & Microscopy, 18-21.
- Wageningen University (2012). Food-Info.net website, http://www.food-info.net/uk/carbs/starch.htm.
- Wang, L. F., Wang, Y. J., & Porter, R. (2002). Structures and physicochemical properties of six wild rice starches. *Journal of Agricultural and Food Chemistry*, 50(9), 2695-2699.
- Whistler, R. L., ed (1964). *Methods in carbohydrate chemistry*. New York and London: Academic Press.
- Wikipedia (2006). Extrusion webpage, http://en.wikipedia.org/wiki/Extrusion.
- Wilson, R. H., Goodfellow, B. J., Belton, P. S., Osborne, B. G., Oliver, G., & Russell, P. L. (1991). Comparison of Fourier-Transform mid infrared-spectroscopy and near-infrared reflectance spectroscopy with differential scanning calorimetry for the study of the staling of bread. *Journal of the Science of Food and Agriculture*, 54(3), 471-483.
- Zeleznak, K. J., & Hoseney, R. C. (1986). The role of water in the retrogradation of wheat-starch gels and bread crumb. *Cereal Chemistry*, 63(5), 407-411.
- Zhuang, H. N., An, H. Z., Chen, H. Q., Xie, Z. J., Zhao, J. W., Xu, X. M., & Jin, Z. Y. (2010). Effect of extrusion parameters on physicochemical properties of hybrid indica rice (type 9718) extrudates. *Journal of Food Processing and Preservation*, 34(6), 1080-1102.

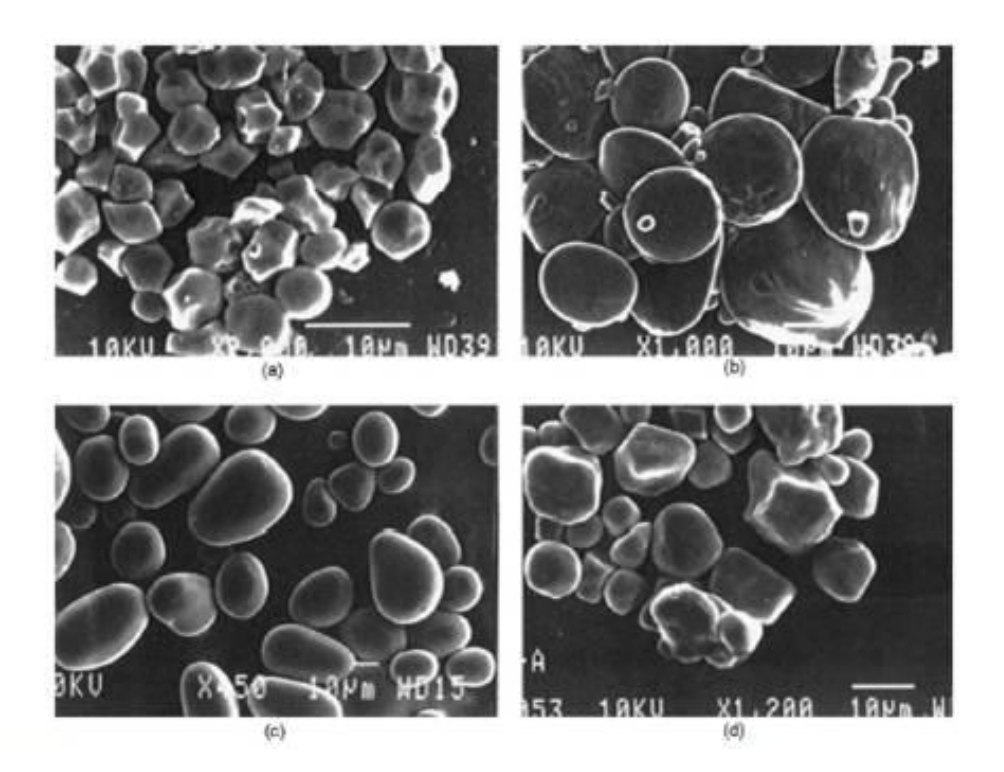


Figure 2.1. Scanning electron micrographs of starches separated from different sources. (a) rice, (b) wheat, (c) potato, (d) corn (bar = $10 \mu m$). (Singh et al., 2003)

Table 2.1. Characteristics of starch granules from different botanical sources. (Tester et al., 2004)

Starch	Type	Shape	Distribution	Size (µm)
Barley	Cereal	Lenticular (A-type), spherical (B-type)	Bimodal	15-25, 2-5
Maize (waxy and normal)	Cereal	Spherical/polyhedral	Unimodal	2-30
Amylomaize	Cereal	Irregular	Unimodal	2-30
Millet	Cereal	Polyhedral	Unimodal	4-12
Oat	Cereal	Polyhedral	Unimodal	3-10 (single)
				80 (compound)
Pea	Legume	Rentiform (single)	Unimodal	5-10
Potato	Tuber	Lenticular	Unimodal	5-100
Rice	Cereal	Polyhedral	Unimodal	3-8 (single)
				150 (compound)
Rye	Cereal	Lenticular (A-type)	Bimodal	10-40
		Spherical (B-type)		5-10
Sorghum	Cereal	Spherical	Unimodal	5-20
Tapioca	Root	Spherical/lenticular	Unimodal	5-45
Triticale	Cereal	Spherical	Unimodal	1-30
Sago	Cereal	Oval	Unimodal	20-40
Wheat	Cereal	Lenticular (A-type)	Bimodal	15-35
		17.5	Spherical (B-type)	2-10

Adapted from Tester and Karkalas (2002).

Amylose: α -(1 \rightarrow 4)-glucan; average n = ca. 1000. The linear molecule may carry a few occasional moderately long chains linked α -(1 \rightarrow 6).

Figure 2.2. Chemical structure of amylose. (Tester et al., 2004)

Amylopectin:
$$\alpha$$
-(1 \rightarrow 6) branching points. For exterior chains a = ca. 12-23. For interior chains b = ca. 20 - 30. Both a and b vary according to the botanical origin.

Figure 2.3. Chemical structure of amylopectin. (Tester et al., 2004)

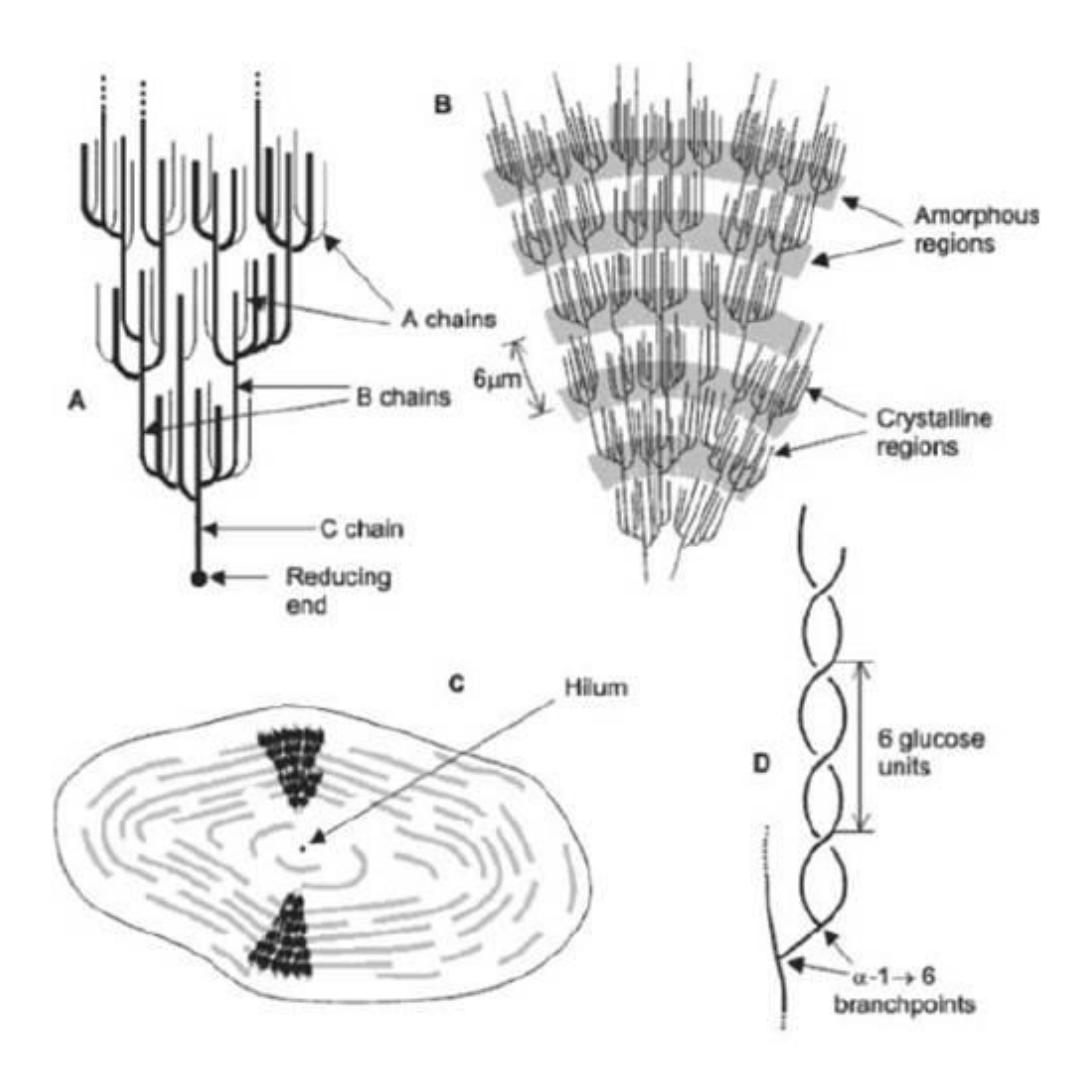


Figure 2.4. Structure of starch. (a) Shows the essential features of amylopectin. (b) Shows the organization of the amorphous and crystalline regions (or domains) of the structure generating the concentric layers that contribute to the "growth rings" that are visible by light microscopy. (c) Shows the orientation of the amylopectin molecules in a cross section of an idealized entire granule. (d) Shows the likely double helix structure taken up by neighboring chains and giving rise to the extensive degree of crystallinity in granule (www.lsbu.ac.uk). (Sajilata et al., 2006)

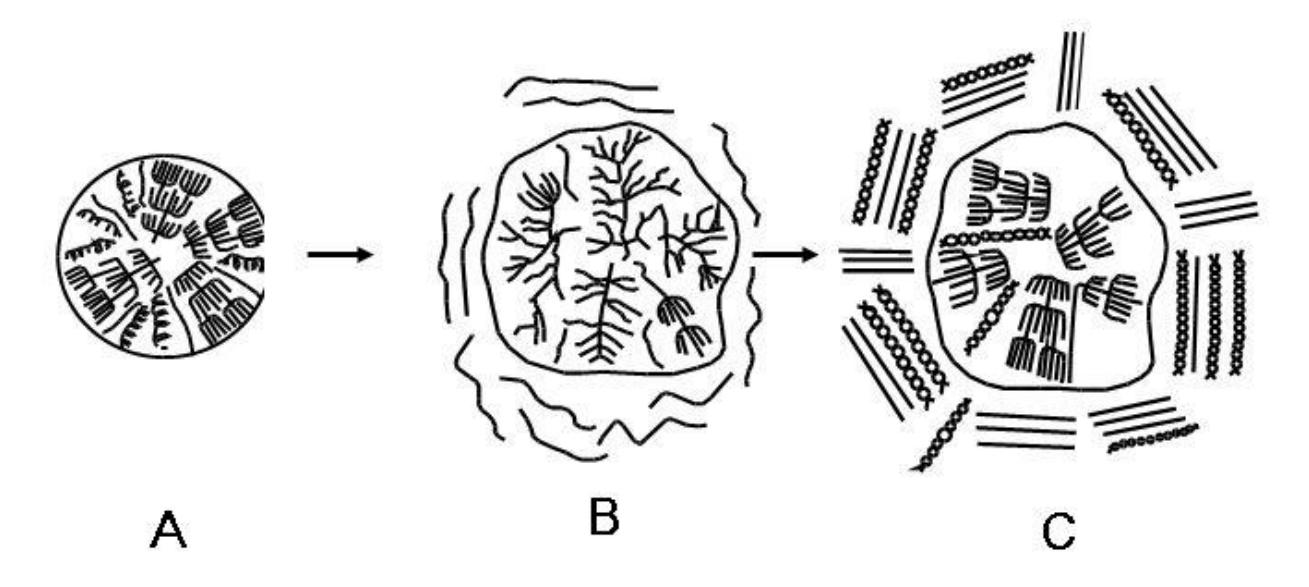


Figure 2.5. Gelatinization and retrogradation of starch. (A) Native starch, (B) Gelatinized starch, (C) Retrograded starch. (Wageningen University, 2012)

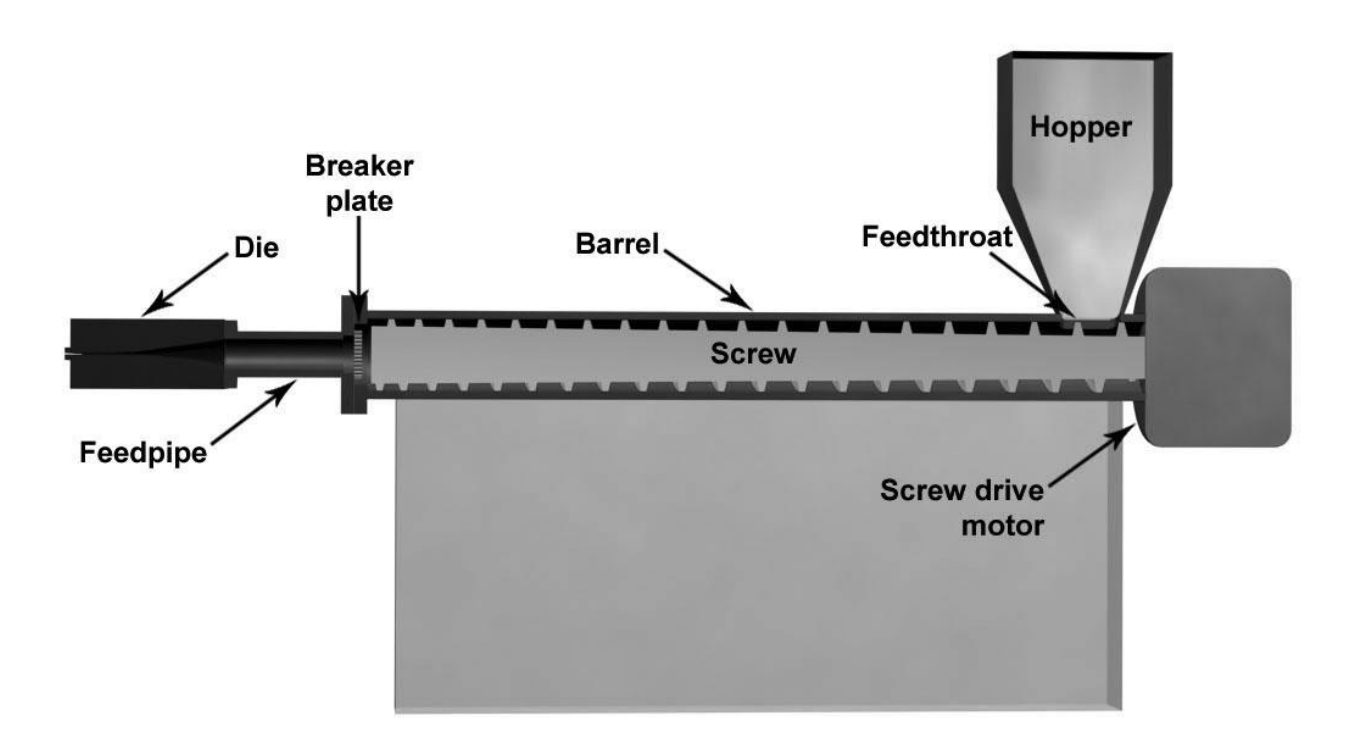


Figure 2.6. Diagram of an extruder. Material moves down the screws from the hopper towards the die, where expansion takes place. (Wikipedia, 2006)

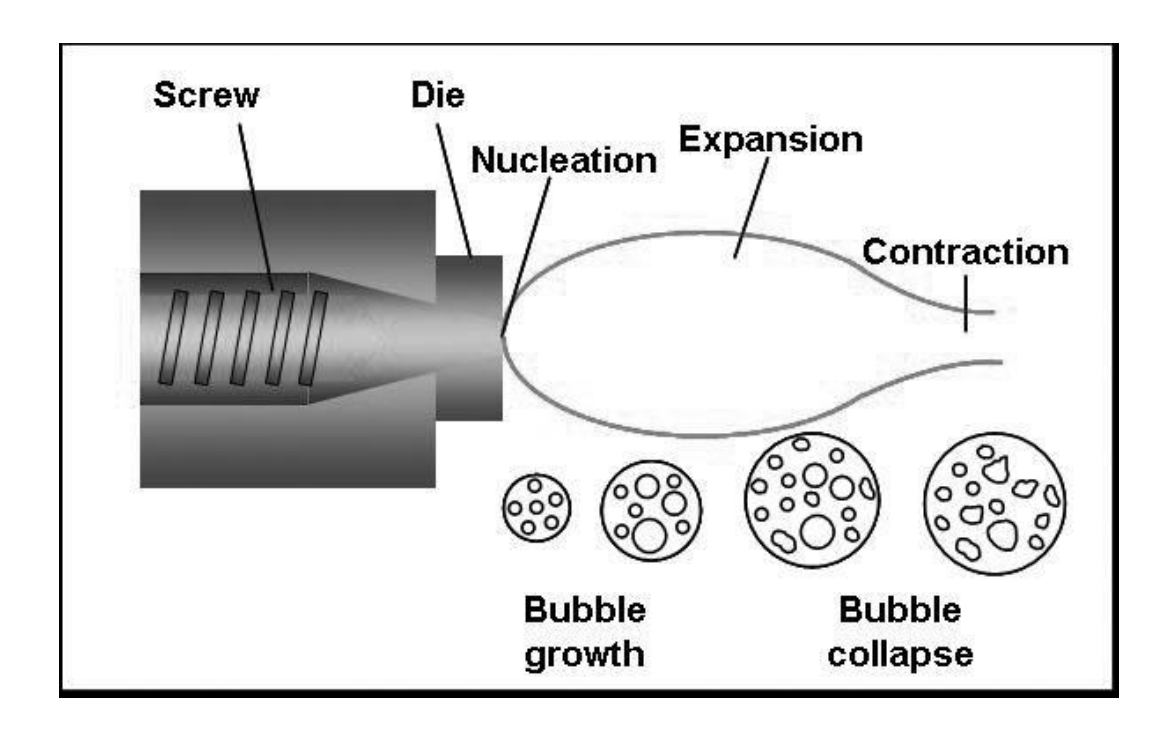


Figure 2.7. Diagram of the expansion process during extrusion. (Moraru et al., 2003)

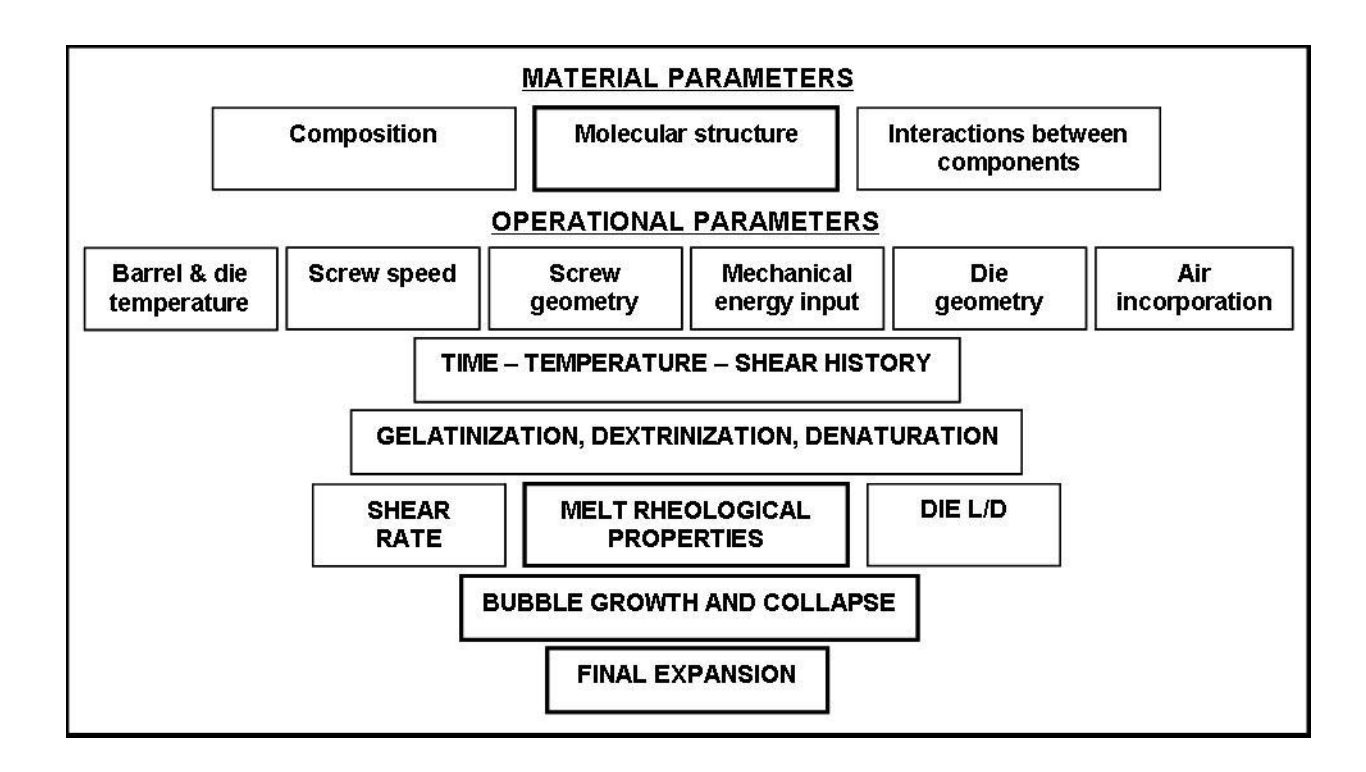


Figure 2.8. Main factors influencing expansion during extrusion. (Stevens et al., 1995)

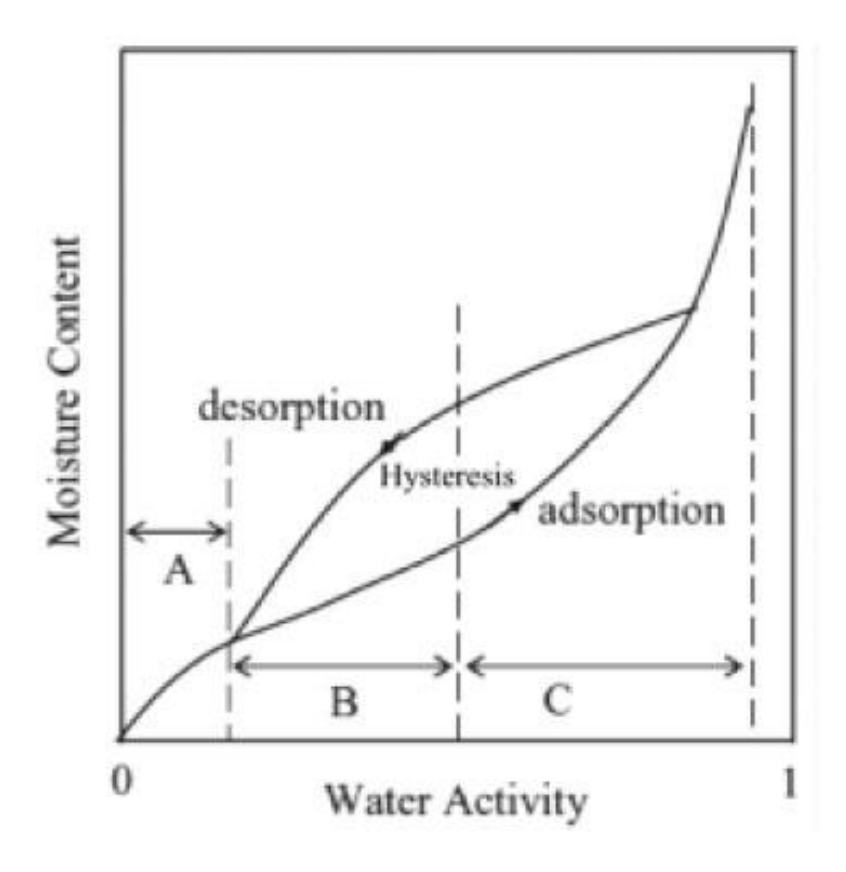


Figure 2.9. Sorption isotherm for the typical food product. A) Monolayer; B) Multilayer; C) Liquid or free water. Hysteresis = difference between adsorption and desorption isotherm. (Andrade et al., 2011)

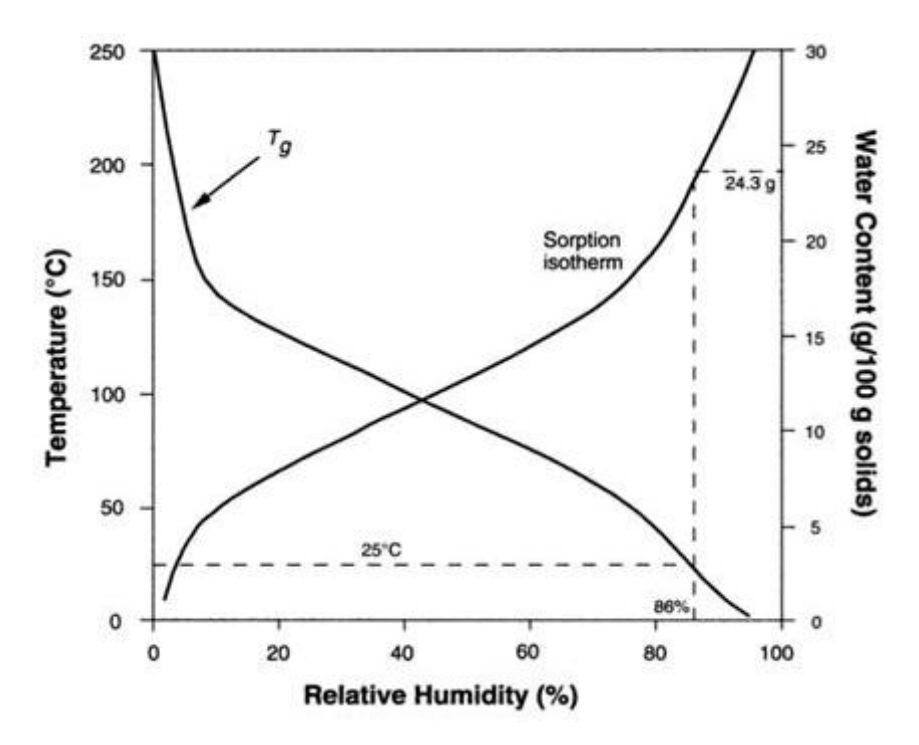


Figure 2.10. Overlay of sorption isotherm and plasticizing effect of water on $T_{\rm g}$ of starch.

 T_g -labeled curve is a plot of glass transition temperatures based on relative humidity. (Jouppila et al., 1997)

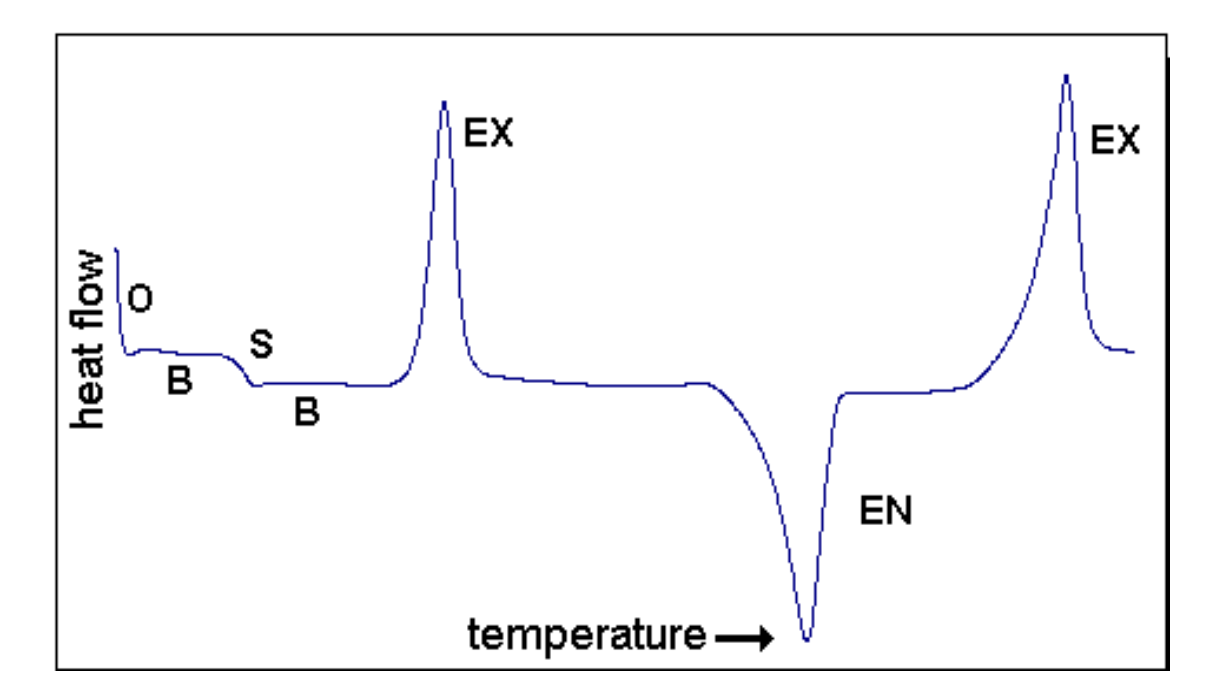


Figure 2.11. General diagram of a DSC curve. O = Offset generally observed at the beginning of heating; B = Baseline; S = Step change that occurs when a change in heat capacity is observed without a discrete enthalpy change; EX = Exothermic peak; EN = Endothermic peak. (Anasys, 2012)

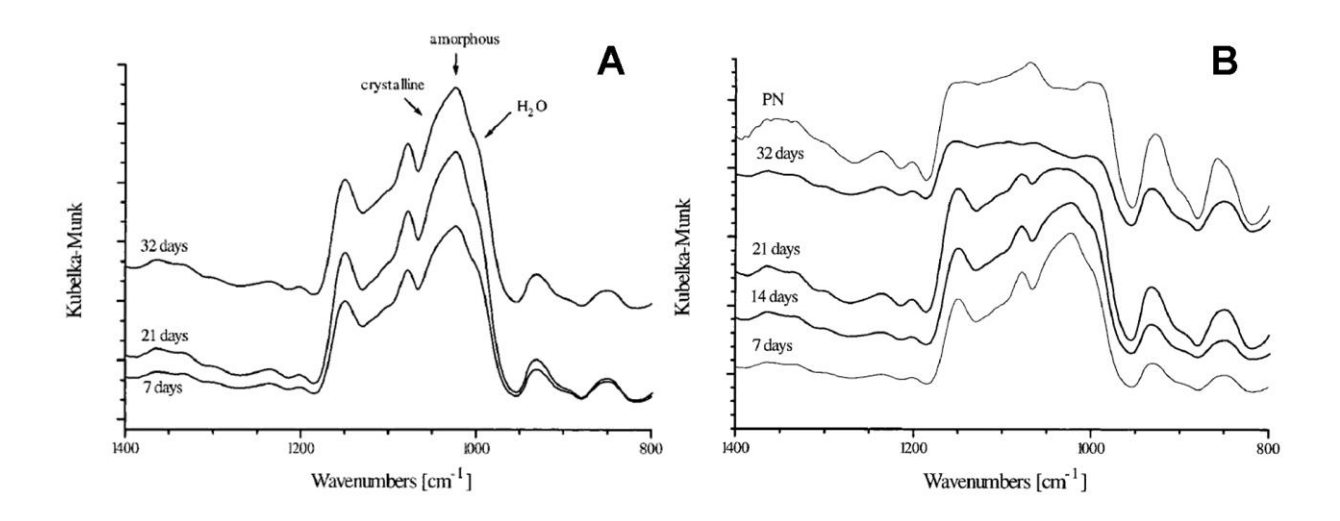


Figure 2.12. FTIR spectra of freeze-dried gelatinized native potato starch (PN). (A) FTIR spectra of freeze dried gelatinized PN stored for 7, 21 and 32 days at 20 °C and 30% RH; **(B)** FTIR spectra of freeze dried gelatinized PN stored for 7, 14, 21 and 32 days at 20 °C and 90% RH, and of native potato starch PN. (Smits et al., 1998)

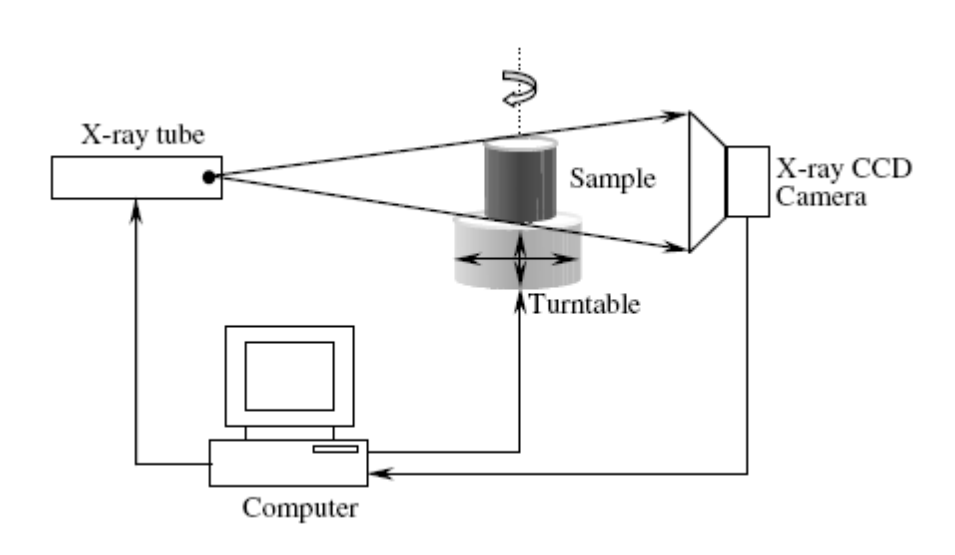


Figure 2.13. Schematic diagram of X-ray microcomputed tomography. (Lim et al., 2004)

Table 2.2. Spin of nuclei used for NMR. (Hornak, 1997-9)

Nuclei	Unpaired Protons	Unpaired Neutrons	Net Spin
¹ H	1	0	1/2
² H	1	1	1
³¹ P	1	0	1/2
²³ Na	1	2	3/2
¹⁴ N	1	1	1
¹³ C	0	1	1/2
¹⁹ F	1	0	1/2

CHAPTER 3

STARCH EXTRUDATE STRUCTURE MEASURED BY MICRO-CT DURING STORAGE¹

¹ Castlejohn, C.A., Cavendar, G.A., Lin, A.S., Hawkins, S.A. and L. Wicker. To be submitted to *Carbohydrate Polymers*.

Abstract

Microcomputed Tomography (microCT), a three-dimensional imaging technique, was

used to study density differences in expanded maize starch extrudates during 8 weeks of storage.

The pore network showed a similar spatial distribution throughout storage, but minor changes in

structure were detected through analysis of the raw imaging data even though DSC and FTIR did

not indicate that retrogradation occurred. The raw data was analyzed to determine the %

porosity, the % pore interconnectivity, and the mean and median pore diameter at weeks 0, 4,

and 8. Most of the changes in the pores were observed between weeks 0 and 4 with an increase

in the % porosity (29.1% to 33.7%), an increase in the % pore interconnectivity (93.9% to

98.9%), and a shift in the pore diameter distribution. Although retrogradation was undetectable

using analytical methods, structural changes suggest that early retrogradation might be occurring

or that moisture migration might be responsible. Small volumes of high density areas were

distributed within the solid material in the extrudate, but no trends were observed over the time

course of storage, and the composition of these areas remains unknown. MicroCT detected an

increase in the porosity and an increase in the amount of and decrease in the density of high

density areas 4 hours and 24 hours after compression during cutting. These data suggest

relaxation of the extrudate was still occurring during this time period and illustrate the

importance of consistency in the timing of imaging.

Keywords: X-ray tomography; MicroCT, starch, extrusion, pores

Introduction

The food industry generates many different products from extrusion of starch-based materials, including pasta, cereal, pet food, and snack foods. The snack food industry has expanded greatly in recent years, and as more and more extruded starch products are being generated, more understanding of the changes occurring during storage of these products is needed. In previous years, the understanding of the changes during storage has primarily been provided through the use of analytical techniques, such as Differential Scanning Calorimetry (DSC) and Fourier Transform Infrared Spectroscopy (FTIR). As useful as analytical techniques are in providing information about the staling process, these methods do not provide a visual representation of the changes during storage. Images of these extrudates during storage could better illustrate structural and localized changes that are occurring during storage providing a more complete picture of why the changes detected by analytical methods decrease product quality. In addition, some of these imaging techniques may prove to be more sensitive to quality changes during storage due to their high resolution.

Conventional imaging methods used for studying extruded starch products include light microscopy (Chaudhary, Torley, Halley, McCaffery & Chaudhary, 2009; Enrione, Hill & Mitchell, 2007; Salmenkallio-Marttila, Heinio, Myllymaki, Lille, Autio & Poutanen, 2004), polarized light microscopy (Altan, McCarthy & Maskan, 2009; Bhatnagar & Hanna, 1996; Mousia, Farhat, Pearson, Chesters & Mitchell, 2001), and electron microscopy (Batterman-Azcona, Lawton & Hamaker, 1999; Dean, Do, Petinakis & Yu, 2008; Lopez-Rubio, Flanagan, Shrestha, Gidley & Gilbert, 2008; Lopez-Rubio, Htoon & Gilbert, 2007; Ma, Yu & Ma, 2005; Mahasukhonthachat, Sopade & Gidley, 2010; Majdzadeh-Ardakani & Nazari, 2010; Simmons &

Thomas, 1995; Ushakumari, Latha & Malleshi, 2004; Zhuang et al., 2010), but these methods are each limited in their own way.

Light microscopy is quick and inexpensive, but staining is usually required to distinguish different structures. Polarized light microscopy is useful for detecting ungelatinized starch granules, but is limited in the types of structures that are detectable. Both scanning electron microscopy (SEM) and transmission electron microscopy (TEM) provide excellent resolution, but are expensive methods with intricate, time-consuming preparation methods. All of these imaging methods are limited to 2-D cross sections of the material or to imaging of surface structures only. In addition, most of these techniques require destruction of the sample for imaging.

Microcomputed tomography (microCT) is a useful imaging technique that uses emission of X-rays through a rotating object to first generate 2-D tomograms that are then processed based on differences in radiodensity within the object to render 3-D images (Lim & Barigou, 2004). This method can not only detect differences between the solid material and the pores, but can also detect density differences within the solid material to help in imaging internal structures. This technique is quick, requires no sample preparation, and is relatively inexpensive when compared to electron microscopy. In addition, microCT is a non-destructive technique, so the same sample can be used for additional testing, both analytical and imaging.

Computed tomography is widely used in the medical industry to generate images, but has only recently started to be used at a smaller scale for imaging food. Most of these studies have focused on using X-ray tomography to determine characteristics of the porosity in a wide range of food items, such as ice cream (Pinzer, Medebach, Limbach, Dubois, Stampanoni & Schneebeli, 2012), fried chicken nuggets (Adedeji & Ngadi, 2009; Adedeji & Ngadi, 2011),

baked goods (Esveld, van der Sman, van Dalen, van Duynhoven & Meinders, 2012; Lim et al., 2004), and cereals (Chaunier, Della Valle & Lourdin, 2007; Guessasma, Chaunier, Della Valle & Lourdin, 2011; van Dalen, Blonk, van Aalst & Hendriks, 2003). Previous microCT studies on starch extrudates have not used this technique to observe changes during storage, but rather to provide useful information about differences in the structure of these extrudates based on differences in starting material and extrusion conditions (Babin, Della Valle, Dendievel, Lourdin & Salvo, 2007; Plews, Atkinson & McGrane, 2009). Babin et al. (2007) compared textural differences in extrudates of similar relative densities with different wall thicknesses and pore sizes and found that those with smaller wall thickness and pore size were more resistant to rupture. Plews et al. (2009) measured the porosity of extrudates using microCT and found the results comparable to gravimetric methods as well as using this method to determine how interconnected the pores were within extrudates of different amounts of expansion. The goal of this study is to use microCT to observe and characterize structural changes occurring during storage of extruded starch.

Material and Methods

Starch Extrusion

Melojel maize starch (Batch# DAK3125) was obtained courtesy of National Starch, LLC (Bridgewater, NJ). Based on product information from National Starch, Melojel is a native maize starch with ~25% amylose content, <0.5% protein content, and <0.15% lipid content. Extrusion of the maize starch-water mixture was performed using an MPF30 co-rotating twin-screw extruder (APV Baker, Ltd., Grand Rapids, MI). The screw configuration consisted of wide forward flight (1.5D) feed screws with a mixing block consisting of 5 kneading blocks at the

point of entry of the Type II deionized water pumped in from a Bran+Leubbe® metering pump (Buffalo Grova, IL) to allow for good mixing of the starch and water. Starch was fed into the extruder at a rate of 74 g/min (150 rpm feeder rate) and conveyed down the co-rotating screws with a screw speed of 280 rpm out a 4mm circular die at the end of the barrel. Deionized water was pumped into the barrel at a rate resulting in ~45% moisture content during the extrusion and ~27% moisture after expansion and cooling. A temperature of 80°C was maintained throughout the barrel during extrusion. The product showed controlled expansion to a diameter of 6±1 mm from the 4 mm die. The extrudate was cooled for 1 hour at room temperature and then sliced using a scalpel to individual pieces of ~6 cm in length for storage.

Storage conditions

The starch extrudates were stored at 4°C for 8 weeks in a vacuum-sealed desiccator with potassium nitrate (CAS# 7757-79-1, J. T. Baker Chemical Co., Phillipsburg, NJ) saturated salt solution made with Type II deionized water providing a high moisture environment (96% RH) and refrigeration temperatures to promote staling of starch via moisture migration and retrogradation and to slow microbial growth.

Moisture and Water Activity

The moisture content of the extrudate was determined by comparing the weight of a sample (~200 mg) before and after drying in a vacuum oven (381 mm Hg) at 130°C overnight. The water activity was determined using an AquaLab water activity meter (Decagon Devices, Inc., Pullman, WA). Moisture content and water activity were measured on the day of extrusion (Week 0) and during weeks 2, 4 and 8 of storage. All measurements were performed in triplicate.

Sorption Isotherm

A random sample of the starch extrudate was ground prior to measuring the sorption isotherm. Some of the ground sample was put aside for FTIR analysis, but the ground sample to be used for measuring the sorption isotherm was stored in an airtight container with Drierite to shorten the drying period prior to measuring the sorption isotherm (W. A. Hammond Drierite Co. Ltd., Xenia, OH).

The sorption isotherm was measured at 23°C using an IGAsorp Sorption Isotherm Analyzer (Hiden Isochema, Warrington, WA). The isotherm was obtained using a small sample (~100 mg) over a 50 hour period that consisted of an initial 8 hour drying period at 0% RH followed by 2-4 hours each for equilibration at 10 subsequent relative humidities (5, 15, 25, 35, 45, 55, 65, 75, 85, and 93% RH). Moisture content was measured throughout the equilibration process and reported after equilibration had occurred at the selected relative humidities. The sorption isotherm analysis was performed in triplicate.

The data were fit using the Guggenheim, Anderson, and de Boer (GAB) regression model for sorption isotherms. The equation (1) is as follows:

$$m = \frac{Ckm_0 a_W}{(1 - ka_W)(1 - ka_W + Cka_W)} \tag{1}$$

With m being the moisture content, a_w being the water activity, C and k being energy constants, and m_0 being the moisture content at the monolayer capacity.

Differential Scanning Calorimetry (DSC)

DSC was performed on 5-10 mg samples of the starch extrudate using a DSC Star^e System DSC1 (Mettler Toledo, Inc., Columbus, OH). Each sample was sealed in a standard 40 µL aluminum pan (ME-27331, Mettler Toledo, Inc., Columbus, OH) and compared to an empty

reference pan. The pans were heated from 20-200°C at 10°C/min. The thermograms were analyzed using software provided by Mettler Toledo. Samples were tested in triplicate during weeks 0, 2, 4 and 8.

Fourier Transform Infrared Spectroscopy (FTIR)

FTIR spectra were measured on ground extrudate samples using a Nicolet 6700 FTIR (Thermo-Scientific, West Palm Beach, FL). The spectra were measured from 4000-700 cm⁻¹ using an Attenuated Total Reflection (ATR) accessory (Durascope, Smiths Detection, Danbury, CT) with a diamond crystal and 64 scans per spectrum. The intensities of two particular peaks were examined: the peak corresponding to crystalline starch (1037 cm⁻¹) and the peak corresponding to amorphous starch (1014 cm⁻¹) (Fig. 3.1). The ratio of the crystalline to the amorphous peak was calculated for each spectrum before an average was obtained to eliminate the need for baseline correction and normalization between spectra. FTIR spectra were measured on the day of extrusion (Week 0) and during weeks 2, 4, and 8 of storage. All measurements were performed in triplicate.

MicroCT

MicroCT imaging was performed on starch extrudate samples during weeks 0, 4, and 8 of storage. Samples used for imaging were visually selected to have similar shapes and sizes. Both ends of the starch extrudates were removed by using a scalpel to slice in the transverse direction to a final length of ~1.5 cm. The samples were placed in 7mm sample tubes that were sealed with parafilm. Due to the compression that occurred during the cutting process, the samples were allowed to relax for 24 hours in the sealed sample tube prior to microCT imaging. During week

4, an additional image was taken 4 hours after cutting (on the same sample) to determine the effects of compression on the extrudate.

A 1mm section of the starch extrudate samples were scanned with a μ CT50 system (Scanco Medical, Bruttisellen, Switzerland) in the 7mm sample tubes at 4 μ m voxel size. Source and detector settings were as follows: E = 55kVp, I = 109uA, power = 6W, integration time = 1000ms, pixel matrices 2048x2048. Raw data were automatically reconstructed to 2-D grayscale slice tomograms using a cone beam convolution backprojection algorithm. Materials within the starch composites were thresholded using global segmentation to separate higher density material, lower density material, and air. The resulting 3-D binarized images were used to compute material volumes, radiodensity in the form of linear attenuation, pore diameters, and pore size distributions. Thickness measurements were taken at each voxel using an expanded spheres method of analysis.

Results and Discussion

Moisture Analysis

The moisture content in the extrudates remained relatively constant throughout storage with the moisture content ranging between 27.3% and 29.3% moisture. The water activity of the starch extrudate was 0.92±0.00 just after extrusion and remained at 0.94±0.01 throughout the 8 weeks of storage. These results suggest that storage conditions were stable throughout the study. The water activity that was maintained throughout storage was in the area of the sigmoid sorption isotherm (data not shown) that indicates the presence of free or liquid water in the extrudate (Andrade, Lemus & Perez, 2011). The presence of free water in the extrudate during storage should promote moisture migration, a common cause of quality loss in extruded starch

(Bourlieu, Guillard, Powell, Valles-Pamies, Guilbert & Gontard, 2008; Choi, Ahn, Choi, Hwang, Kim & Baik, 2008; Roca, Guillard, Guilbert & Gontard, 2006). In addition, the high water activity should promote retrogradation (recrystallization) of starch, the major cause of staling and quality loss in starch-based materials, at 4°C based on the mechanics of nucleation and crystallization (Jouppila & Roos, 1997).

Retrogradation Analysis

Retrogradation of amylopectin, the highly branched component of starch, is the most common cause of staling in starch-based products as it occurs over a long period of time causing long term changes in texture. Retrogradation is typically studied using analytical methods with two of the quickest and most commonly used being DSC and FTIR. DSC results showed a small peak ($\Delta H = -0.195 \text{ J/g}$) at $78.8\pm1.05^{\circ}\text{C}$ just after extrusion, indicating a trace amount of ungelatinized starch granules in the extrudate, but this peak was undetectable in subsequent weeks of storage. However, no peak corresponding to amylopectin retrogradation, which can be found between 40°C and 100°C , was observed during storage (Abd Karim, Norziah & Seow, 2000; Eerlingen, Jacobs & Delcour, 1994; Sievert & Pomeranz, 1989).

FTIR results also found no evidence that retrogradation occurred during storage. The ratio of the intensities of the crystalline starch peak (1037 cm⁻¹) to the amorphous starch peak (1014 cm⁻¹) has been shown to shift towards one as retrogradation of starch occurs (Abd Karim et al., 2000; Smits, Ruhnau, Vliegenthart & van Soest, 1998). No difference was observed in the ratios of the crystalline to amorphous peaks in the FTIR spectra throughout storage (Table 3.1). These results suggest that even though storage conditions were designed to promote retrogradation, little to no retrogradation was detectable using analytical methods.

Pore Distribution During Storage

MicroCT can easily detect the difference between solid material and air space based on their differences in density. The raw imaging data can be analyzed at different thresholds to characterize each component of a material. This method was used to observe and characterize changes in the pores during storage. There was no visible difference in the distribution of the pores throughout 8 weeks of storage, and pores were evenly distributed throughout the extrudate (Fig. 3.2). An obvious bubble can be seen in the image of the extrudate in Week 8. The data from this bubble were removed from analyses to prevent the mean pore diameter and the pore size distribution from being skewed. With this adjustment, little to no change was observed in the mean and median pore diameters throughout storage (Table 3.2).

Even though little to no difference was observed in these values during storage, there was an increase in the % porosity. The % porosity is the portion of the total volume that does not consist of solid material. A percentage was used to eliminate differences due to fluctuations in the size of the extrudate. This increase in the % porosity reflected an overall increase in the number of pores during storage rather than an increase in the size of the pores as no difference was observed in the mean and median pore diameters. A noticeable shift was observed in the pore diameter distribution throughout storage from a higher to a lower percentage of the mean pore size and a slight widening of the distribution in the percentage at either side of the base of the peak (Fig. 3.3). Again, a percentage was used to eliminate differences due to differences in the sample size of the extrudate, The decrease in the percentage of the mean pore diameter does not reflect a decrease in the number of these pores as the % porosity increased during storage, but rather a decrease in their percentage of the total pore volume. As the peak in the pore diameter

distribution only became flatter and wider rather than shifting, the mean pore diameter showed only a minor increase during storage.

A network of interconnected pores was present as the % pore interconnectivity was >90% throughout the study. An increase in the percentage of porosity and the percentage of interconnected pores in the imaged area was observed between Week 0 and Week 4, but little change was observed between Week 4 and Week 8. These data indicate that most of the changes in the pores occurred during the first 4 weeks of storage and that there was a general increase in the size and scope of the pore network during storage. This change should allow increased moisture migration, which would lead to an increase in quality loss via texture changes.

The changes observed in the pores show some basic structural changes occurring during storage that would be unobservable using other methods. Although DSC and FTIR results suggested that retrogradation did not occur, the changes in pore characteristics suggest that some staling mechanism was at work during storage. There is a possibility that the changes observed in the pore network were due to moisture migration instituting minute textural changes via swelling or plasticization or perhaps these changes were due to small changes occurring during early stages of retrogradation via nucleation and limited growth of crystallites that were undetectable by other analytical methods.

Pores After Cutting/Compression

Because microCT is a quick, non-destructive imaging method unlike most other imaging methods, it can easily be used to observe structural changes in a sample at short time intervals. For preparation of the samples for imaging, both ends of the extrudate were removed using a scalpel to slice in the transverse direction causing compression of the sample. During Week 4 of

storage, images of the same sample were produced at two different times after the compression that occurred during the cutting process (4 hours and 24 hours post-cutting). The sample was sealed with parafilm in the imaging tube, which should prevent any major loss of moisture between the imaging times.

No noticeable difference was observed in the distribution of the pores throughout the extrudate (data not shown), but several differences were seen in the analysis of the raw data (Table 3.3). Within the 20-hour period between images, there was an increase in the percentage of porosity and the percentage of pores that were interconnected, showing an expansion of the pore network. In addition, there was a decrease in the mean and median pore diameters, and a noticeable shift was observed in the pore diameter distribution between the two imaging times (Fig. 3.4), showing an increase in the percentage of smaller pore sizes.

Because these data were observed in such a short period of time eliminating staling as a mechanism for these changes and because the moisture loss during this time period was limited, these changes were probably the result of relaxation of the pore network after the compression that occurred during cutting. As more of the smaller pores relaxed, the porosity and interconnectivity increased while the percentage of smaller pore diameters increased. These data show the importance of allowing time for relaxation to occur before imaging and being consistent in the time of imaging after cutting. One limitation when using such a high resolution during microCT imaging is that effects of either moisture loss or relaxation that may be undetectable at lower resolutions are capable of creating detrimental motion artifacts at high resolution. This study used 4µm resolution as a compromise between obtaining a high resolution and limiting artifacts from low signal:noise ratios in higher resolutions.

High Density Material

Although microCT is typically used to distinguish the pores from the solid material in starch extrudates, it can be used to detect areas of different density within the material. In addition to the density difference between the solid material and the pores, higher density areas were observed within the solid material in this study. The general distribution of these high density areas is shown in Figs. 3.5 and 3.6. These images are representative of those seen throughout the storage study showing the distribution of the high density areas concentrated towards the center of the starch extrudate and the distribution of the high density areas in relation to the pores in a cross-section.

The raw imaging data for the high density areas was analyzed to determine their percentage of the solid material and their density. The high density areas ranged from 0.2% - 0.6% of the total solid material throughout the study, but no trend was evident during storage. The differences observed were probably due to heterogeneity within the product. However, a difference was observed in the high density areas in the images generated at 4 hours and 24 hours after cutting the extrudate. In the 20-hour interim between images of the same sample, the high density volume increased from 0.2% to 0.6 % of the total volume, while the density of the high density areas dropped 32%. These changes were probably due to relaxation after compression for the aforementioned reasons and again illustrate the importance of consistency in the timing of image generation throughout the storage.

The composition of the high density areas remains undetermined. Little to no retrogradation occurred based on DSC and FTIR results although some early retrogradation via nucleation and minimal growth of crystallites may have occurred that was undetectable at the sensitivity of these methods. However, because these high density areas were observed within 24

hours after extrusion and the amounts of these high density areas should have been detected by DSC if these areas were composed of retrograded starch, it is unlikely the high density areas are composed of retrograded starch.

Based on the low percentage of the total volume that consists of the high density areas, a few different possibilities exist. DSC indicated that there were trace amounts of ungelatinized starch just after extrusion. Ungelatinized starch granules are semi-crystalline, so they could conceivably have enough of a density difference to be resolved by microCT. However, the peak corresponding to ungelatinized starch disappeared by Week 2 of storage, so the data do not support their persistence throughout storage making it unlikely that they compose the high density areas.

Lipids are known to form complexes with amylose, which are visible in X-ray diffraction patterns using Wide-angle X-ray Scattering (Abd Karim et al., 2000; Singh, Gamlath & Wakeling, 2007). The lipid content of the starch is <0.15%, but there is a possibility that this value could increase if lipid-amylose complexes were formed during the extrusion process. Another option is that these high density areas consist of the protein found in the starch, which makes up <0.5% of the total content of the starch. These high density inclusions were assumed to be protein in a previous study of starch extrudates, but no methods have been used to confirm their identity (Plews et al., 2009). There is a possibility that as the proteins denatured during the extrusion process, exposed lysine groups may have formed conjugates with the free glucose and starch molecules contributing to the range of sizes seen in these high density areas in Fig. 3.6 (Singh et al., 2007). Further studies could focus on determining the content of these high density areas, possibly through differential staining of thin sections of starch extrudates.

Conclusions

MicroCT is a powerful technique for quantitatively assessing porous starch extrudates during storage. The changes observed during storage were very small size-scale morphological and compositional variations in the porous and solid structures that would be difficult to observe using 2-D imaging methods and analytical techniques. In addition, this method uncovered minor changes that occurred due to compression that would be nearly impossible to quantify with other methods. Future studies could increase the sample size for imaging by using multiple samples from different regions of the extrudate to examine localized effects or micro-environments, increase storage time to allow for additional staling, or try to correlate structural changes observed using microCT to changes in texture and physical properties. This method could then be applied to determine changes that lead to quality loss and lead to extension of the shelf-life of these products.

References

- Abd Karim, A., Norziah, M. H., & Seow, C. C. (2000). Methods for the study of starch retrogradation. *Food Chemistry*, 71(1), 9-36.
- Adedeji, A. A., & Ngadi, M. O. (2009). 3-D Imaging of Deep-Fat Fried Chicken Nuggets

 Breading Coating Using X-Ray Micro-CT. *International Journal of Food Engineering*,

 5(4).
- Adedeji, A. A., & Ngadi, M. O. (2011). Microstructural characterization of deep-fat fried breaded chicken nuggets using x-ray micro-computed tomography. *Journal of Food Process Engineering*, 34(6), 2205-2219.
- Altan, A., McCarthy, K. L., & Maskan, M. (2009). Effect of Extrusion Cooking on Functional Properties and in vitro Starch Digestibility of Barley-Based Extrudates from Fruit and Vegetable By-Products. *Journal of Food Science*, 74(2), E77-E86.
- Andrade, R. D., Lemus, R., & Perez, C. E. (2011). Models of sorption istherms for food: Uses and limitations. *Vitae-Revista De La Facultad De Quimica Farmaceutica*, 18(3), 324-333.
- Babin, P., Della Valle, G., Dendievel, R., Lourdin, D., & Salvo, L. (2007). X-ray tomography study of the cellular structure of extruded starches and its relations with expansion phenomenon and foam mechanical properties. *Carbohydrate Polymers*, 68(2), 329-340.
- Batterman-Azcona, S. J., Lawton, J. W., & Hamaker, B. R. (1999). Effect of specific mechanical energy on protein bodies and alpha-zeins in corn flour extrudates. *Cereal Chemistry*, 76(2), 316-320.
- Bhatnagar, S., & Hanna, M. A. (1996). Starch-stearic acid complex development within single and twin screw extruders. *Journal of Food Science*, 61(4), 778-782.

- Bourlieu, C., Guillard, V., Powell, H., Valles-Pamies, B., Guilbert, S., & Gontard, N. (2008).

 Modelling and control of moisture transfers in high, intermediate and low a(w) composite food. *Food Chemistry*, 106(4), 1350-1358.
- Chaudhary, A. L., Torley, P. J., Halley, P. J., McCaffery, N., & Chaudhary, D. S. (2009).

 Amylose content and chemical modification effects on thermoplastic starch from maize
 Processing and characterisation using conventional polymer equipment. *Carbohydrate*Polymers, 78(4), 917-925.
- Chaunier, L., Della Valle, G., & Lourdin, D. (2007). Relationships between texture, mechanical properties and structure of cornflakes. *Food Research International*, 40(4), 493-503.
- Choi, Y. J., Ahn, S. C., Choi, H. S., Hwang, D. K., Kim, B. Y., & Baik, M. Y. (2008). Role of Water in Bread Staling: A Review. *Food Science and Biotechnology*, 17(6), 1139-1145.
- Dean, K. M., Do, M. D., Petinakis, E., & Yu, L. (2008). Key interactions in biodegradable thermoplastic starch/poly(vinyl alcohol)/montmorillonite micro- and nanocomposites. *Composites Science and Technology*, 68(6), 1453-1462.
- Eerlingen, R. C., Jacobs, H., & Delcour, J. A. (1994). Enzyme-resistant starch. 5. Effect of retrogradation of waxy maize starch on enzyme susceptibility. *Cereal Chemistry*, 71(4), 351-355.
- Enrione, J. I., Hill, S. E., & Mitchell, J. R. (2007). Sorption and diffusional studies of extruded waxy maize starch-glycerol systems. *Starch-Starke*, *59*(1), 1-9.
- Esveld, D. C., van der Sman, R. G. M., van Dalen, G., van Duynhoven, J. P. M., & Meinders, M.
 B. J. (2012). Effect of morphology on water sorption in cellular solid foods. Part I: Pore scale network model. *Journal of Food Engineering*, 109(2), 301-310.

- Guessasma, S., Chaunier, L., Della Valle, G., & Lourdin, D. (2011). Mechanical modelling of cereal solid foods. *Trends in Food Science & Technology*, 22(4), 142-153.
- Jouppila, K., & Roos, Y. H. (1997). The physical state of amorphous corn starch and its impact on crystallization. *Carbohydrate Polymers*, 32(2), 95-104.
- Lim, K. S., & Barigou, M. (2004). X-ray micro-computed tomography of cellular food products. Food Research International, 37(10), 1001-1012.
- Lopez-Rubio, A., Flanagan, B. M., Shrestha, A. K., Gidley, M. J., & Gilbert, E. P. (2008).

 Molecular rearrangement of starch during in vitro digestion: Toward a better understanding of enzyme resistant starch formation in processed starches.

 Biomacromolecules, 9(7), 1951-1958.
- Lopez-Rubio, A., Htoon, A., & Gilbert, E. P. (2007). Influence of extrusion and digestion on the nanostructure of high-amylose maize starch. *Biomacromolecules*, 8(5), 1564-1572.
- Ma, X. F., Yu, J. G., & Ma, Y. B. (2005). Urea and formamide as a mixed plasticizer for thermoplastic wheat flour. *Carbohydrate Polymers*, 60(1), 111-116.
- Mahasukhonthachat, K., Sopade, P. A., & Gidley, M. J. (2010). Kinetics of starch digestion and functional properties of twin-screw extruded sorghum. *Journal of Cereal Science*, *51*(3), 392-401.
- Majdzadeh-Ardakani, K., & Nazari, B. (2010). Improving the mechanical properties of thermoplastic starch/poly(vinyl alcohol)/clay nanocomposites. *Composites Science and Technology*, 70(10), 1557-1563.
- Mousia, Z., Farhat, I. A., Pearson, M., Chesters, M. A., & Mitchell, J. R. (2001). FTIR microspectroscopy study of composition fluctuations in extruded amylopectin-gelatin blends. *Biopolymers*, 62(4), 208-218.

- Pinzer, B. R., Medebach, A., Limbach, H. J., Dubois, C., Stampanoni, M., & Schneebeli, M. (2012). 3D-characterization of three-phase systems using X-ray tomography: tracking the microstructural evolution in ice cream. *Soft Matter*, 8(17), 4584-4594.
- Plews, A. G., Atkinson, A., & McGrane, S. (2009). Discriminating Structural Characteristics of Starch Extrudates through X-ray Micro-tomography using a 3-D Watershed Algorithm.

 International Journal of Food Engineering, 5(1).
- Roca, E., Guillard, V., Guilbert, S., & Gontard, N. (2006). Moisture migration in a cereal composite food at high water activity: Effects of initial porosity and fat content. *Journal of Cereal Science*, 43(2), 144-151.
- Salmenkallio-Marttila, M., Heinio, R. L., Myllymaki, O., Lille, M., Autio, K., & Poutanen, K. (2004). Relating microstructure, sensory and instrumental texture of processed oat. Agricultural and Food Science, 13(1-2), 124-137.
- Sievert, D., & Pomeranz, Y. (1989). Enzyme-resistant starch. 1. Chracterization and evaluation by enzymatic, thermoanalytical, and microscopic methods. *Cereal Chemistry*, 66(4), 342-347.
- Simmons, S., & Thomas, E. L. (1995). Structural characteristics of biodegradable thermoplastic starch/poly(ethylene-vinyl alcohol) blends. *Journal of Applied Polymer Science*, *58*(12), 2259-2285.
- Singh, S., Gamlath, S., & Wakeling, L. (2007). Nutritional aspects of food extrusion: a review.

 International Journal of Food Science and Technology, 42(8), 916-929.
- Smits, A. L. M., Ruhnau, F. C., Vliegenthart, J. F. G., & van Soest, J. J. G. (1998). Ageing of starch based systems as observed with FT-IR and solid state NMR spectroscopy. *Starch-Starke*, *50*(11-12), 478-483.

- Ushakumari, S. R., Latha, S., & Malleshi, N. G. (2004). The functional properties of popped, flaked, extruded and roller-dried foxtail millet (Setaria italica). *International Journal of Food Science and Technology*, 39(9), 907-915.
- van Dalen, G., Blonk, H., van Aalst, H., & Hendriks, C. L. (2003). 3-D imaging of foods using x-ray microtomography. G. I. T. Imaging & Microscopy, 18-21.
- Zhuang, H. N., An, H. Z., Chen, H. Q., Xie, Z. J., Zhao, J. W., Xu, X. M., & Jin, Z. Y. (2010). Effect of extrusion parameters on physicochemical properties of hybrid indica rice (type 9718) extrudates. *Journal of Food Processing and Preservation*, 34(6), 1080-1102.

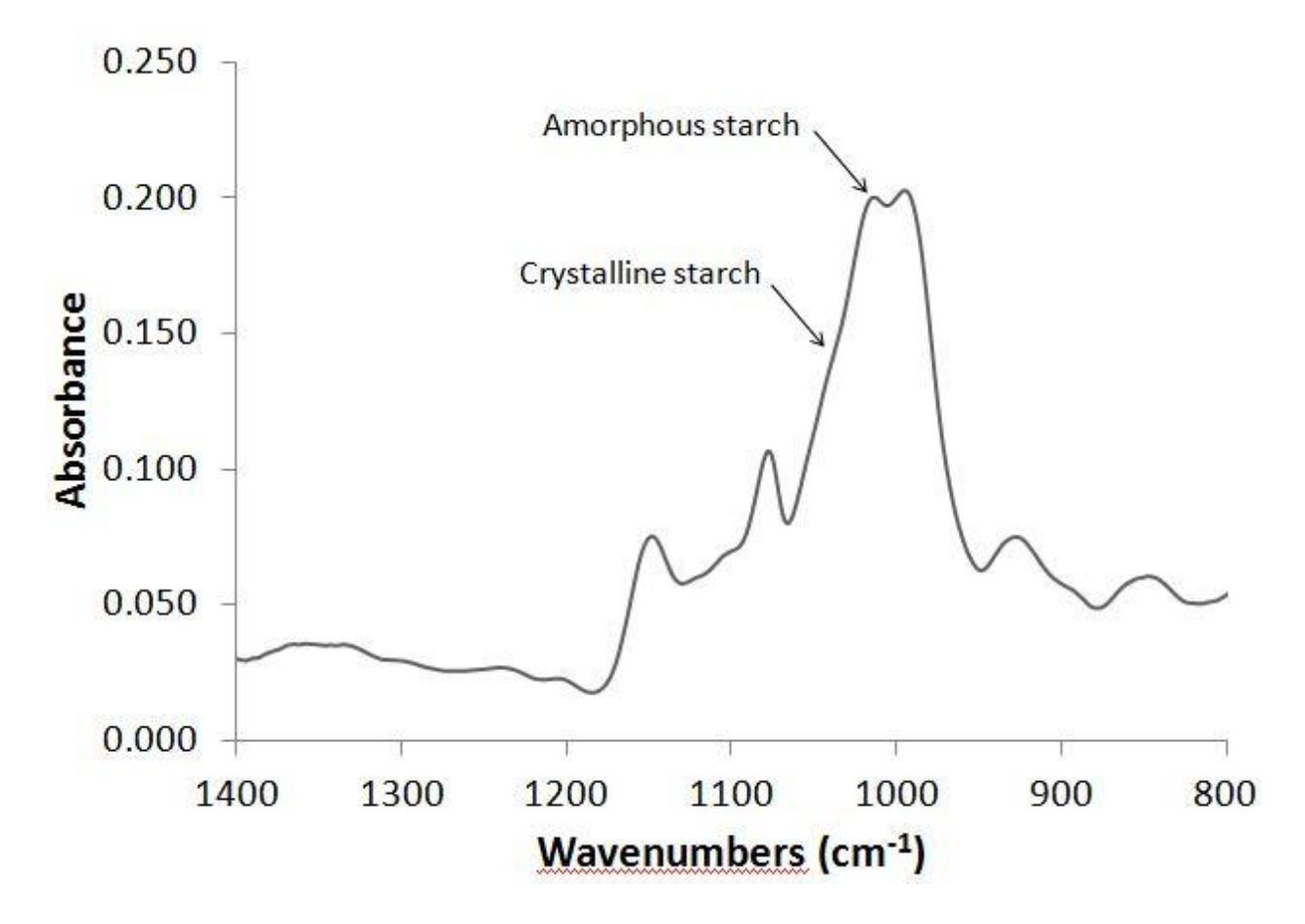


Figure 3.1. FTIR spectrum showing crystalline and amorphous starch peaks.

Table 3.1. Ratios of crystalline to amorphous starch peaks measured by FTIR.

Week of Storage	Crystalline:amorphous peak ratio	
	$(1037 \text{ cm}^{-1}: 1014 \text{ cm}^{-1})$	
0	0.725±0.004	
2	0.718 ± 0.007	
4	0.736 ± 0.011	
8	0.727 ± 0.005	

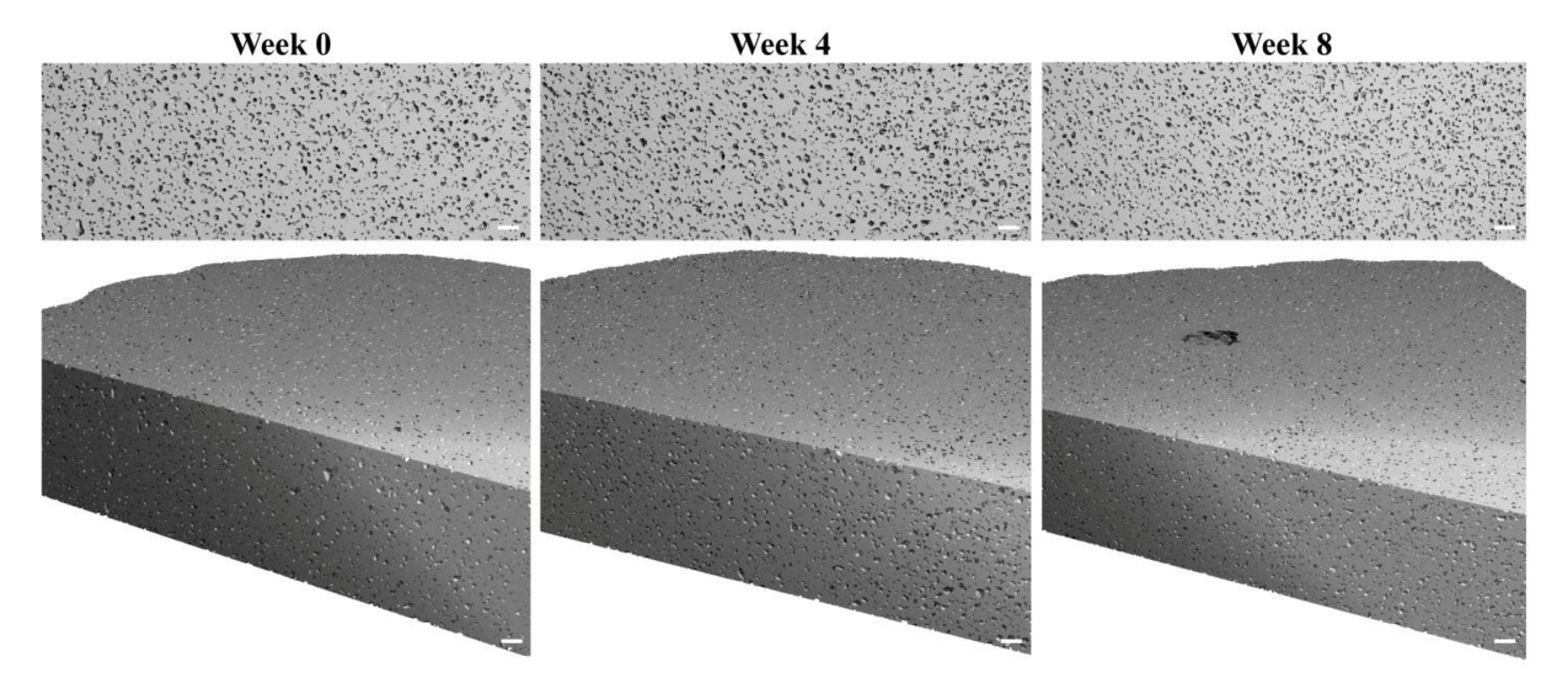


Figure 3.2. Distribution of pores throughout storage. The upper microCT images are of an internal cross-section at Weeks 0, 4, and 8 of storage. The lower microCT images are of the same internal cross section in a 3-D view showing the pore distribution during Weeks 0, 4, and 8. Scale bar = $100 \mu m$.

Table 3.2. Summary of pore characteristics during storage.

	Week 0	Week 4	Week 8 ^a
Mean pore diameter (mm)	0.0173±0.0053	0.0176±0.0055	0.0179 ± 0.0017
Median pore diameter (mm)	0.0160	0.0160	0.0160
% Porosity	29.1	33.7	33.4
% Pore interconnectivity	93.9	98.9	98.7

^a Adjusted values after removal of data related to observed bubble

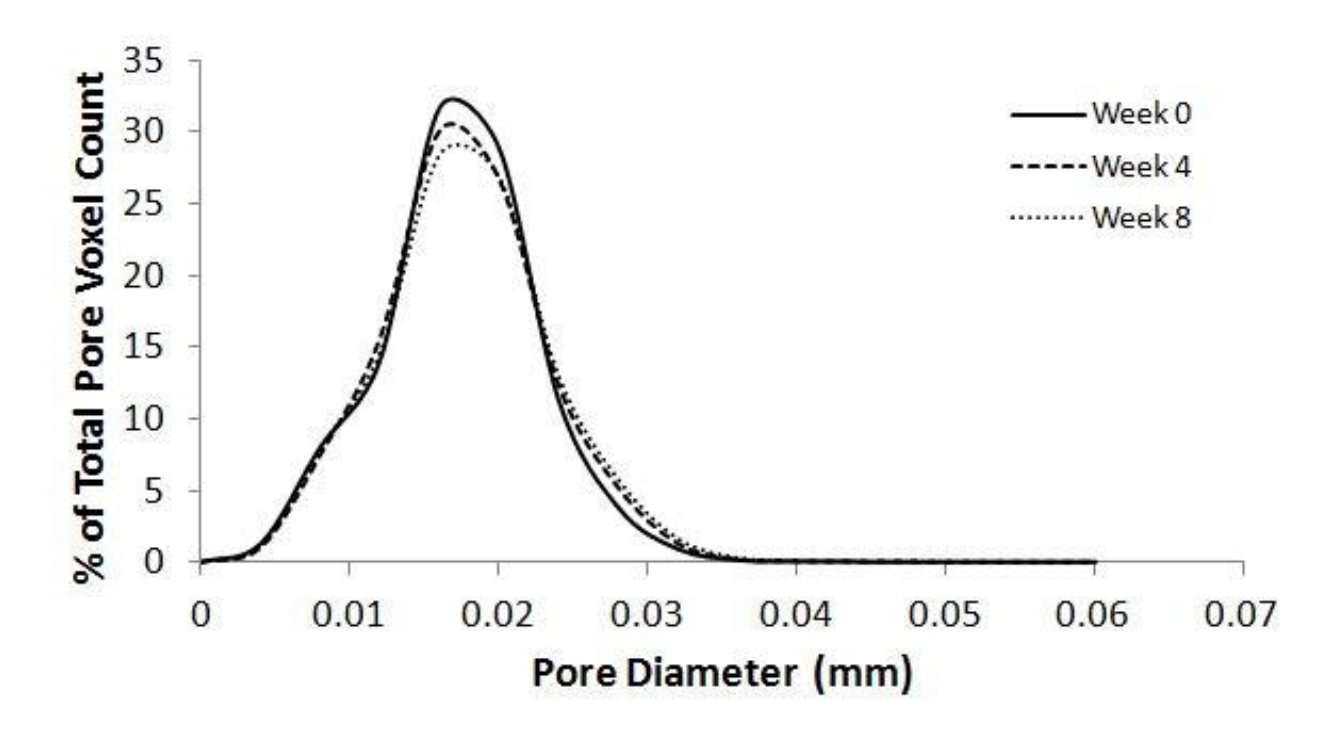


Figure 3.3. Pore diameter distribution during storage.

Table 3.3. Summary of pore characteristics at different times post-cutting during Week 4 of storage.

	4 hours after cutting	24 hours after cutting
Mean pore diameter (mm)	0.0181 ± 0.0060	0.0176 ± 0.0055
Median pore diameter (mm)	0.020	0.016
% Porosity	31.7	33.7
% Pore interconnectivity	98.0	98.9

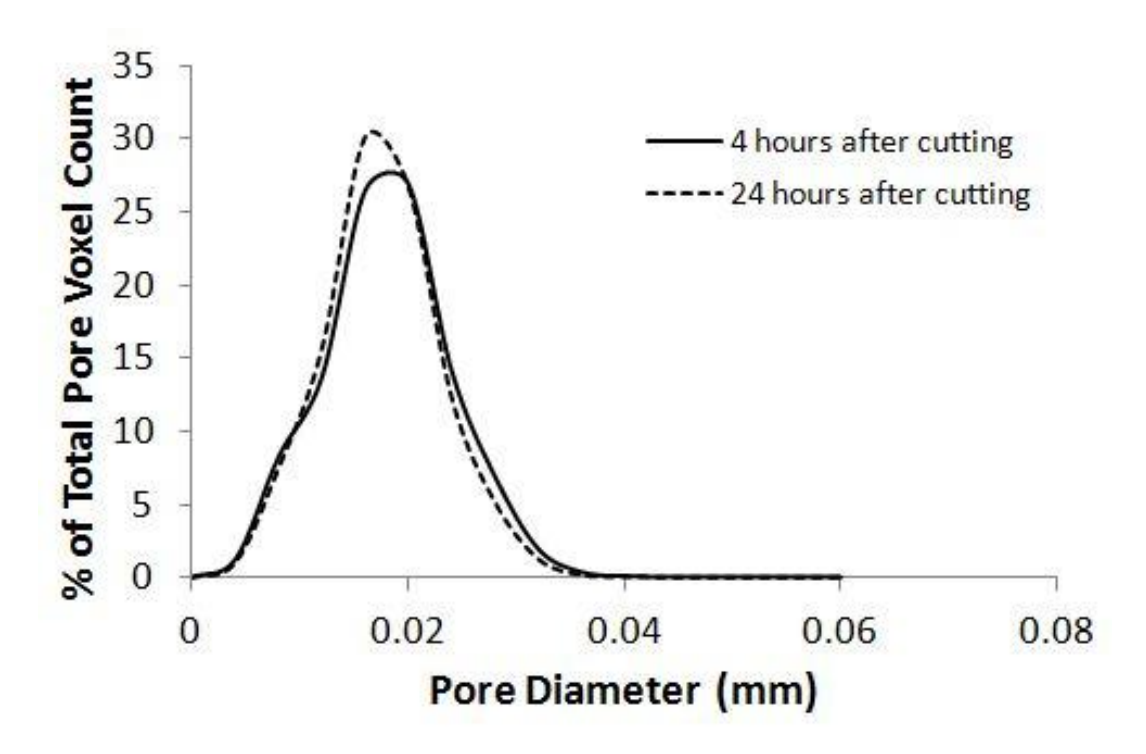


Figure 3.4. Pore diameter distribution at different times post-cutting.

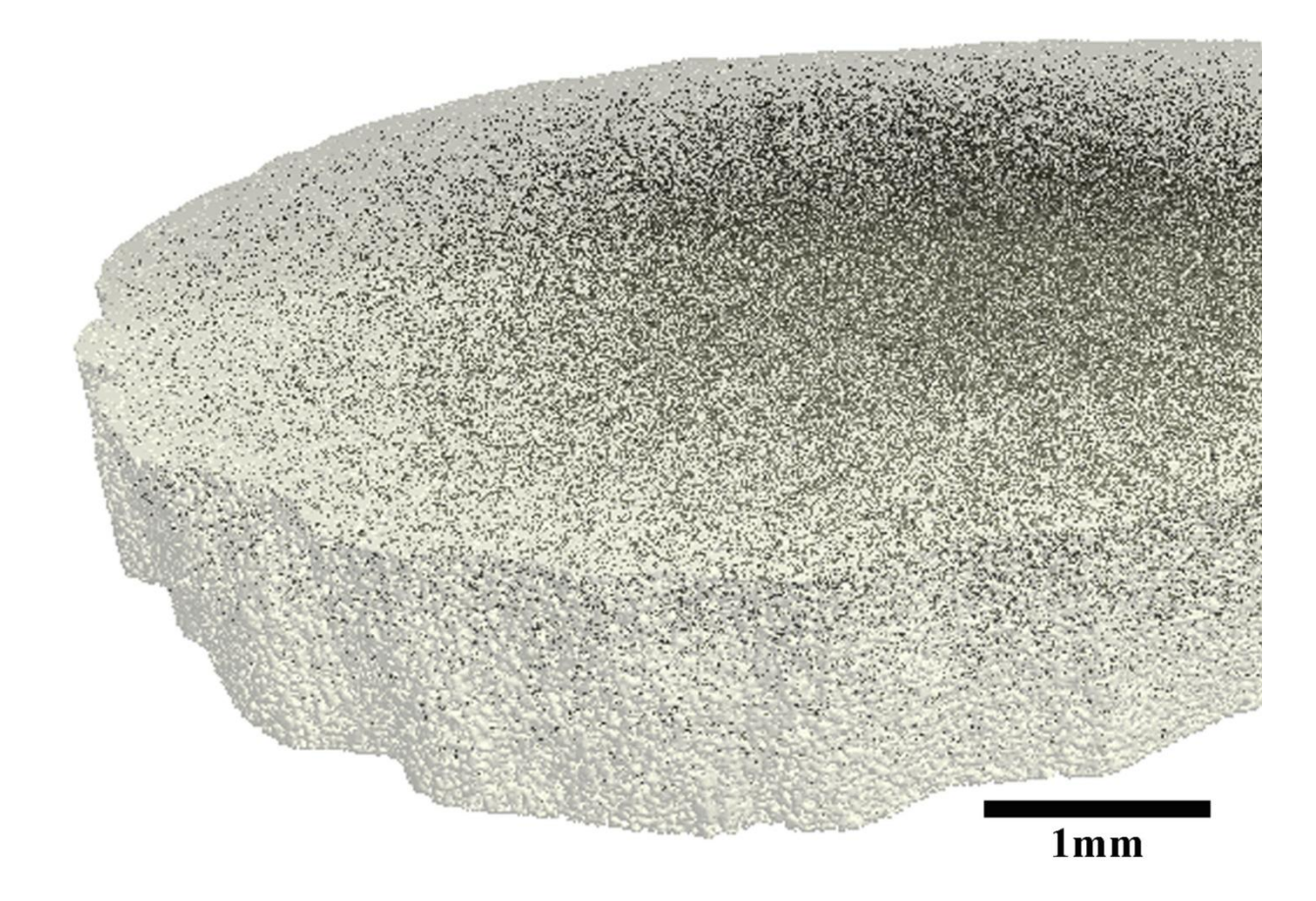


Figure 3.5. 3-D image of distribution of high density material. Higher density material appears darker in this image. This image of the high density material from Week 8 is representative of the distribution seen throughout storage.

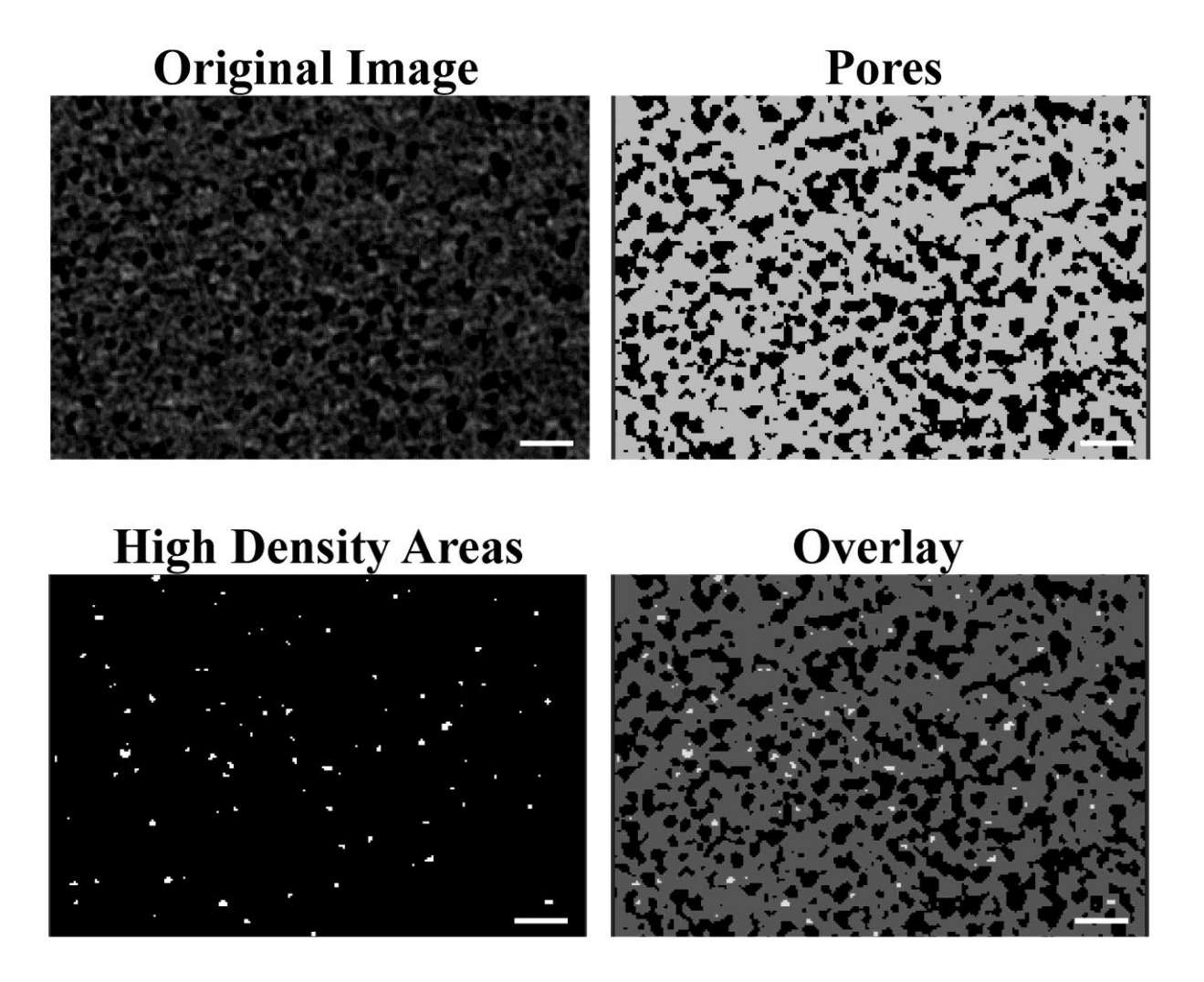


Figure 3.6. 2-D image of distribution of high density material. These images from starch extrudates during Week 8 are representative of those throughout storage. Original Image (10X internal cross-section of the starch extrudate): Higher density materials appear lighter than lower density materials. Pores (Same image with threshold selected to display pores): Pores appear black in color, while solid material appears gray. High Density Areas (Same image with threshold selected to display the high density areas): High density areas appear white, while pores and lower density solid materials appear black. Overlay (High Density Areas image displayed over Pores image): High density areas appear white, lower density material appears gray, and pores appear black. Scale bar = $100 \mu m$.

CHAPTER 4

COMPLEXITY OF CHANGES IN MOISTURE DURING STORAGE OF STARCH ${\sf EXTRUDATES} \ {\sf AS} \ {\sf CHARACTERIZED} \ {\sf BY} \ {\sf MRI}^1$

¹ Castlejohn, C.A., Cavendar, G.A., Leisen, J., Hawkins, S.A. and L. Wicker. To be submitted to *Carbohydrate Polymers*.

Abstract

Magnetic Resonance Imaging (MRI) was used to observe changes in moisture in slightly expanded extruded starch products during 8 weeks of storage within a H₂O or D₂O environment. Some extrudate samples were left intact (Full) and some were bisected (Half). Spin Echo, Single Point Imaging, Spin Density, and T2 images were generated during storage. For simple storage (Full H₂O), an increase in the bound water was observed in the outer edges of the extrudate with more free water retained in the center of the extrudate. However, T2-Weighted images showed the complexity of the moisture changes by showing a difference in the distribution of the free water mobility when compared to the free water concentration observed in the Spin Density images. The extrudates stored in the D₂O environment allowed imaging of the original moisture in the extrudate. The original moisture remained evenly distributed throughout storage even though most of it had left the sample by the Week 8. Images of the Half samples showed that case hardening did affect the overall moisture distribution and the free water mobility during storage.

Keywords: Magnetic Resonance Imaging, starch, extrusion, case hardening, moisture migration

Introduction

Extruded starch products are found throughout many areas of the food industry, such as pasta, cereal, pet food, and snack foods. Production of these types of products, especially snack foods, has increased in recent years. As this industry expands, a greater understanding of changes occurring during storage of these products is necessary.

Moisture, in particular, is a major contributing factor to quality loss in these types of products. As moisture migrates through starch products, localized areas of moisture can cause texture changes due to the plasticizing effects of water and can provide pockets of moisture for microbial growth, both of which effectively decrease the quality and shelf-life of the product (Bourlieu, Guillard, Powell, Valles-Pamies, Guilbert & Gontard, 2008; Choi, Ahn, Choi, Hwang, Kim & Baik, 2008; Kester & Fennema, 1986; Lim & Jane, 1994; Roca, Guillard, Guilbert & Gontard, 2006). To study moisture diffusivity or migration, highly complex, time-consuming methods using drying, water diffusion, and vapor diffusion techniques and modeling are needed, preventing these methods from being widely used in studies of these products (Enrione, Hill & Mitchell, 2007; Zogzas, Maroulis & Marinoskouris, 1994).

In addition to basic moisture migration, extruded products have the additional complication of case hardening. Case hardening, or formation of a hard layer around the outside of the extrudate, can result from some extrusion conditions due to the rapid cooling of the outermost areas of the extruded product during the extrusion process. The edges of the extrudate give up moisture faster than the inside of the extrudate resulting in a hardened surface that can prevent internal moisture from escaping. This hardening of the outer edge of the extrudate can also limit moisture migration into a material providing an additional layer of complexity to an already complex process.

Methods of studying moisture in extruded starch products are typically limited to non-imaging analytical methods, such as moisture content, water activity, and time-consuming sorption isotherms. Some studies incorporate the use of ¹H-NMR, which can provide information about differences in water mobility. However, these analytical techniques do not provide information about changes in the spatial distribution and concentration of the moisture that occur

during storage. Imaging methods are usually used to overcome these limitations in the scope of analytical methods by providing information about the distribution of changes in a material. However, most imaging methods provide structural information about the solids and the pores in a material without having the ability to image moisture. In addition, most of those that can image moisture do not provide information about the mobility of the moisture.

Magnetic Resonance Imaging (MRI) is imaging technique that uses a combination of an applied magnetic field and radio frequency pulses to construct an image of nuclei specific to the frequency used based on detection of their rotating magnetic fields. Different series of pulses can be applied during the imaging process to provide the desired information about the nuclei under study. ¹H-MRI can be used to provide visual images of the distribution, concentration, and mobility of the moisture in a material. Because this technique is quick and non-destructive, the imaged samples can be used for other methods, both imaging and analytical.

MRI is commonly used in the medical industry, but has shown promise in recent years in being applicable to the study of food products. Recent food studies have used this technique to study moisture changes during tempering of rice kernels (Hwang, Cheng, Chang, Lur & Lin, 2009), moisture distributions in blueberries (Gamble, 1994), grains (Himmelsbach & Gamble, 1997), whey protein gels (Oztop, Rosenberg, Rosenberg, McCarthy & McCarthy, 2010), soy protein extrudates (Chen, Wei & Zhang, 2010), and food colloids (Cornillon & Salim, 2000; Mariette, 2009), but these studies did not focus on changes during storage of starch-based materials. Ruan et al. (1996) performed an MRI study of sweet rolls, a porous starch-based baked good, during 5 days of storage. They found a complex relationship occurring between the moisture distribution and the differences in the crumb and crust of the sweet rolls. The moisture distribution shifted from the crumb to the crust during storage, but, conversely, the mobility of

the moisture increased in the center of the crumb during storage. This complex relationship, which was attributed to staling in the rolls due to retrogradation (recrystallization) of starch, suggests that a similar complexity may be occurring in extruded starch products.

One goal of this study is to apply various methods of MRI to observe and characterize changes in the moisture within extruded starch products during storage. Another goal is to follow changes that occurred in the original moisture in the extrudates by storing the extrudates in an environment with deuterium oxide, which is not visible at the frequency used in ¹H-NMR, rather than water. The final goal of this study is to observe and characterize the effects of case hardening on the moisture distribution and mobility during storage.

Materials and Methods

Starch Extrusion

Melojel, a native maize starch containing ~25% amylose, (Batch# DAK3125) was obtained courtesy of National Starch, LLC (Bridgewater, NJ). Extrusion of the maize starch-water mixture was performed as previously described in Chapter 3 using an MPF30 co-rotating twin-screw extruder (APV Baker, Ltd., Grand Rapids, MI). The extrudate had controlled expansion from the 4 mm die to a diameter of 6±1 mm. The extrudate was cooled for 1 hour at room temperature and were then sliced using a scalpel to individual pieces of ~6 cm in length for storage. Half of these extrudates were bisected longitudinally prior to storage to illustrate differences due to case hardening of the extrudates. Those that were not bisected will be referred to as Full extrudates, while those that were bisected will be referred to as Half extrudates.

Storage conditions

The starch extrudates, both Full and Half samples, were stored at 4°C for 8 weeks in 2 vacuum-sealed desiccators with potassium nitrate (CAS# 7757-79-1, J. T. Baker Chemical Co., Phillipsburg, NJ) saturated salt solution providing a high moisture environment (96% RH) and refrigeration temperatures to provide enough moisture for good resolution when imaging, to promote staling of starch via retrogradation and moisture migration, and to slow microbial growth. One desiccator had the salt solution made with Type II deionized water (H₂O) and the other had the salt solution made with deuterium oxide (D₂O, heavy water, CAS# 82-700-01-4, Isotec, Inc., Miamisburg, OH). Since D₂O is not detected at the same frequency as H₂O when using MRI, the two different storage conditions were used to illustrate the changes during storage in the original moisture (storage with D₂O) in the extrudate as compared to all of the moisture (storage with H₂O) in the extrudate.

Moisture and Water Activity

The moisture content and the water activity of the extrudates (both Full and Half) from both storage conditions (H_2O and D_2O) were measured for each treatment as previously described in Chapter 3. Moisture content and water activity were measured on the day of extrusion (Week 0) and during weeks 2, 4 and 8 of storage. All measurements were performed in triplicate.

Sorption Isotherm

A random sample of the starch extrudate (Full stored with H_2O only) was ground prior to measuring the sorption isotherm. The sorption isotherm was measured and fit using the

Guggenheim, Anderson, and de Boer (GAB) model as previously described in Chapter 3. The sorption isotherm analysis was performed in triplicate.

Differential Scanning Calorimetry (DSC)

DSC was performed on 5-10 mg samples of the starch extrudate (Full stored with H_2O only) using a Mettler-Toledo DSC Star^e System DSC1 (Columbus, OH) as described previously in Chapter 3. Samples were tested in triplicate during weeks 0, 2, 4 and 8.

Fourier Transform Infrared Spectroscopy (FTIR)

FTIR spectra were measured on ground extrudate samples (both Full and Half) from both storage conditions (H₂O and D₂O) using a Nicolet 6700 FTIR (Thermo-Scientific, West Palm Beach, FL) as described previously in Chapter 3. FTIR spectra were measured on the day of extrusion (Week 0) and during weeks 2, 4, and 8 of storage. All measurements were performed in triplicate.

Magnetic Resonance Imaging (MRI)

MRI data were recorded on a Bruker DSX400 NMR spectrometer (Bruker BioSpin Corp., Billerica, MA) with Microimaging accessories operating at a magnetic field of 9.4 T (400 MHz 1H frequency). The instrument was operating using Bruker's Paravision software. Samples used for imaging were selected to have similar shapes. The ends were removed from the extrudates (both Full and Half) from both storage conditions (H₂O and D₂O) just prior to imaging to eliminate any possible accumulated moisture at the ends from the storage environment. Samples that were imaged together (Half H₂O and Half D₂O) were separated by

tape, which does not appear in the image, to prevent transfer of moisture between samples. The sample, ranging from 2.5 - 4 cm long, was inserted into a sealed glass tube and axial projections were measured using a 10 mm rf coil. For Spin Echo (SE) experiments due to the short T₂relaxation times of the samples' data, it was necessary to optimize a spin-echo sequence for the use of short echo times (TE). This was achieved by using short rf pulses of 50 and 100 µs, respectively. A 128x128 matrix was recorded for a Field of View of 1 cm. No slice selection was used within the software such that the image represents a projection on the axial plane. The TE was 2.125 ms and the repetition delay (TR) was 2000 ms. For SE, the contrast depends on a variety of factors (TE, TR, T₁-, and T₂-relaxation) along with some artifacts due to experimental conditions (characteristics of the rf coil). An initial image was recorded for this setting. Then a series of images was recorded for 8 subsequent echo times of TE=2.125 ms, 3.625 ms, 5.125 ms, 6.625 ms, 8.125 ms, 9.625 ms, 11.125 ms, 12.625 ms, and 14.125 ms. This series of images was analyzed within the MATLAB® v.7.12.0.635 (2007a, The MathWorks, Natick, MA) programming environment by fitting individual pixel intensities at a position x to an exponential decay according to:

$$I(x) = SD(x) \exp(-TE/T2(x))$$
 (1)

where I(x) is measured contrast, and is measured directly in the SE image. It depends on the following factors: T_2 relaxation time, concentration of spins at position (x), concentration of free water, and instrument settings (such as tuning and the receiver gain). Due to the fact that the minimum measurable TE is > 2 ms, all bound water has relaxed ($T_2 < 500$ microseconds) and only the free water is detected. $SD(x) = c_{free}(x)*cst(x)$, where c_{free} is the concentration of free water, and cst is the instrument constant, which mainly varies based on receiver gain (rg) (optimized for each sample) in the recorded images. Since all instrument parameters were not the

same, cst(x) varies significantly between experiments. Therefore, SD is only a relative measurement for the distribution of c_{free} .

This yielded two parameter-selective images calculated from a series of images to depict physical properties as contrast: SD(x) (Spin Density), which largely reflects the concentration of free water and $T_2(x)$ (T2 Image) reflecting its mobility (i.e., bound state). 2-D Single Point Imaging (SPI) images reflecting the spin-density within the axial projection were also recorded using a pulse length of 20 μ s, a detection time of 300 μ s and a repetition delay of 10 ms. The pixel resolution for these images was 64x64. SPI is a technique designed such that T_2 -relaxation becomes mostly irrelevant, so it reflects the spatial distribution of all 1 H atoms from both free and bound water. MRI images were measured on the day of extrusion (Week 0) and during weeks 2, 4, and 8 of storage.

Results and Discussion

Moisture Analysis

Relatively high moisture was needed in the extrudate to generate a good signal for the MRI images. The moisture content in the extrudates was high enough to provide good signal, but showed minor fluctuations throughout storage with the moisture content at $27.6\pm1.5\%$. The water activity of the starch extrudates was more stable than the moisture content starting at 0.92 ± 0.00 just after extrusion and remaining at 0.94 ± 0.01 throughout the 8 weeks of storage in all samples and storage conditions. No differences were observed among the different treatments (Full vs. Half; H_2O vs. D_2O). These results suggest that storage conditions were reasonably stable throughout the study and that no major changes in the moisture distribution are due to fluctuations in moisture content.

The sorption isotherm provided information on the mobility of the moisture in the extrudates (Fig. 4.1) (Andrade, Lemus & Perez, 2011). The monolayer region of the sorption isotherm can be found at moisture contents below 7.0%, the monolayer value calculated using the GAB model. The sorption isotherm of the material shows a relatively small monolayer region in the portion of the sigmoid curve at low water activity indicating that a small amount of the moisture in the material is tightly bound to the substrate, while the multilayer region in the middle portion of the sigmoid curve is relatively large indicating a larger amount of the moisture in the material is loosely bound. The measured water activity in the extrudates can be found in the free or liquid water portion of the isotherm, indicating the presence of both free and bound water during storage. The presence of free water should promote quality loss via moisture migration, while refrigeration temperatures and high water activity should promote staling via retrogradation (recrystallization) of starch (Jouppila & Roos, 1997).

Retrogradation Analysis

Long-term textural changes observed in starch-based products are mostly attributed to retrogradation of amylopectin, the highly branched component of starch, which recrystallizes slowly. Two of the most common methods for studying retrogradation are DSC and FTIR. DSC, which was only performed on the Full H_2O samples, showed a small peak ($\Delta H = -0.195 \text{ J/g}$) at $78.8\pm1.05^{\circ}\text{C}$ just after extrusion. This peak indicated a trace amount of ungelatinized starch granules in the extrudate, but was undetectable in subsequent weeks of storage. Retrograded amylopectin should produce a peak between 40°C and 100°C during storage, but no peak in that range was observed throughout storage (Abd Karim, Norziah & Seow, 2000; Eerlingen, Jacobs & Delcour, 1994; Sievert & Pomeranz, 1989).

FTIR results found different results for different treatments. As retrogradation of starch progresses, the ratio of the intensities of the crystalline starch peak (1037 cm⁻¹) to the amorphous starch peak (1014 cm⁻¹) has been shown to shift towards one (Abd Karim et al., 2000; Smits, Ruhnau, Vliegenthart & van Soest, 1998). No general trend towards one was observed in the samples stored with H₂O, but the samples stored with D₂O showed a small general increase towards one, indicating that some small amount of retrogradation was detectable in these extrudates (Table 4.1). Although some retrogradation was evident in the D₂O samples, the increase in the FTIR ratio was slight and changes due to recrystallization were unlikely visible at the resolution obtained using MRI but still may be affecting structure at a smaller scale.

MRI Images

MRI images obtained on the day of extrusion (Week 0) and after 8 weeks of storage (Week 8) are depicted (Fig. 4.2). Weeks 2 and 4 are not shown as only minor changes were observed in these images when compared to Week 0. This technique was used to provide images of the moisture in the extrudates, and different methods within this technique were applied using various pulse sequences and means of data analysis to generate different contrast. A description of these methods (SE, SPI, SD, and T2) is given in Table 4.2.

Images of Full H_2O Stored Samples

This storage condition was designed to illustrate accelerated changes in moisture that may occur during long-term storage. The SPI images show that, for both Week 0 and Week 8 of storage, the concentration of all of the water in the extrudate seems to be evenly dispersed throughout the extrudate with the exception of the areas with large bubbles, which are circular in

appearance and appear either lighter from containing more water or darker from lack of water. However, a difference is noticeable when comparing the concentration of all of the water (SPI images) with the concentration (SD images) and concentration and mobility (SE images) of the free water only. Areas of high and low free water concentration and mobility are visible in images from all weeks, but the differences between these regions are more pronounced in Week 8. More free water is located towards the center of the extrudates throughout storage, while less free water is generally seen in the outer edge of the noodle. Therefore, even though the outer edge and the center of the extrudate show similar total water concentrations, the outer edge shows less free water indicating the presence of more bound water in these areas.

T2 images reflect a physical property, which is indicative of the mobility of free water. Therefore, images can be compared to one another making T2 images extremely useful when comparing extrudates from different weeks of storage. When comparing the free water mobility from Week 0 to Week 8, a noticeable drop in the relaxation time, or free water mobility, is evident in the outer edges in Week 8 even though the moisture content and total water distribution are similar, again indicating an increase in the proportion of bound water in the outer edges of the extrudates. Interestingly, the area of higher free water mobility in Week 8 (T2 Image) does not correspond to the area of higher free water concentration as seen in the SD image from Week 8. Even though the free water is concentrated along the left side of the extrudate, the free water mobility is highest in the center of the extrudate surrounded by a ring of lower free water mobility.

These results point to a high degree of complexity in the relationship of the moisture to the surrounding environment during storage as seen in other starch-based products (Ruan et al., 1996). Previous studies have suggested that a major reason for this complexity is the relationship

between the moisture and retrograded starch, which may expel moisture from the starch matrix as recrystallization occurs leading to an increase in free water (Whistler & Daniel, 1985) or may trap moisture within the crystalline structure during recrystallization leading to a decrease in the mobility of the water (Leung, Magnuson & Bruinsma, 1983). In this study, the moisture content and the water activity were similar throughout storage and no evidence for retrogradation during storage was observed by DSC or FTIR for these samples. However, a previous study of these extrudates (Chapter 3) showed changes in the pore network during storage that may have been due to early stages of retrogradation undetectable by DSC and FTIR or moisture migration. The expansion of the pore network that was observed during storage should increase the ability of the moisture in the extrudates and the surrounding environment to migrate. These results suggest a probable relationship between the moisture migration and changes in the pore network during storage. In addition, the area of free water mobility within the center of the extrudate is similar to the distribution of high density material of unknown composition seen in Chapter 3, suggesting a possible relationship between the two.

Images of D_2O Stored Samples

This storage condition was used to illustrate changes that occurred only in the original moisture in the extrudates because D₂O is not imaged at the same frequency as H₂O. Some obvious differences in the quality of the SE and SPI images can be seen when comparing to the Full D₂O images to Full H₂O images. This decrease in quality is due to the lower amount of signal in these extrudates. One can also note that even though the signal is much lower, the intensity in the image is similar to the Full H₂O images demonstrating that these images should not be compared to each other in a quantitative manner.

For the SE, SPI, and SD images, no obvious differences were observed between the distributions in the Full D_2O images and those in Full H_2O images. These results suggest that the original moisture retained in the extrudate stayed fairly evenly distributed throughout the extrudate during storage and that the D_2O vapor easily penetrated into the extrudates. T2 images show major increases in T_2 -relaxation time. These results can be explained by the lack of signal in these samples. T_2 -relaxation is given by the dipolar coupling between neighboring 1H -atoms. Therefore, T2 is not only an indication of the mobility of 1H moieties, but also of their (average) distance. Introduction of 2H dilutes the overall pool of 1H and 2H , so the average distance between 1H sites gets larger. The dipolar coupling gets larger and T_2 -relaxation times are increased. Even though the relaxation times are skewed by the D_2O , there still seems to be a less obvious central core of higher relaxation time or higher free water mobility as seen in the Full H_2O images

Side-by-side images of the Half samples allows comparison of the differences between storage with D₂O and H₂O as these samples were imaged at the same length and used the same imaging parameters. The SE, SPI, and SD images all show the obvious difference in the H₂O signal that was not as clear when comparing two different images. These images confirm that there was some moisture exchange with the surrounding environment occurring during storage, with most of the original moisture leaving the Half D₂O sample by Week 8. Since the T₂-relaxation times for the Full D₂O and Half D₂O samples are similar, this indicates that the full D₂O samples also lost most of their original moisture by Week 8.

The Half Both images also allow us to study the effects of case hardening on the moisture distribution as part of the extrudate was exposed without the case intact. A comparison of T2 images showed slightly lower relaxation times for the split samples compared to the full samples.

This indicates that case hardening did have some effect on lowering the overall free water mobility. In addition, the distribution of this free water mobility changed during storage as free water mobility was more evenly distributed in the Half samples as compared to the Full samples. Although no obvious difference in seen in the images comparing free water distribution (SE images), the T2 images and the SD images do indicate a change in the free water distribution as well as in the free water mobility.

Conclusions

This study shows that complex changes occur in the distribution of free and bound water and free water mobility during storage of starch extrudates. MRI proved to be a useful technique for studying moisture changes in these extrudates. MRI, a quick, non-destructive technique, can provide in-depth information about changes in the distribution, concentration, and mobility of the moisture that are unavailable using other methods. This technique is also useful in determining changes in the distribution of free and bound water within a product. The complexity of the changes in the moisture in the starch extrudates during storage could not have been obtained without an imaging technique and the combination of the various methods available when using MRI. In particular, T2 imaging shows promise as a useful method for comparing materials throughout a storage study due to the comparability on the same scale of one image to the next.

References

- Abd Karim, A., Norziah, M. H., & Seow, C. C. (2000). Methods for the study of starch retrogradation. *Food Chemistry*, 71(1), 9-36.
- Andrade, R. D., Lemus, R., & Perez, C. E. (2011). Models of sorption istherms for food: Uses and limitations. *Vitae-Revista De La Facultad De Quimica Farmaceutica*, 18(3), 324-333.
- Bourlieu, C., Guillard, V., Powell, H., Valles-Pamies, B., Guilbert, S., & Gontard, N. (2008).

 Modelling and control of moisture transfers in high, intermediate and low a(w) composite food. *Food Chemistry*, 106(4), 1350-1358.
- Chen, F. L., Wei, Y. M., & Zhang, B. (2010). Characterization of water state and distribution in textured soybean protein using DSC and NMR. *Journal of Food Engineering*, 100(3), 522-526.
- Choi, Y. J., Ahn, S. C., Choi, H. S., Hwang, D. K., Kim, B. Y., & Baik, M. Y. (2008). Role of Water in Bread Staling: A Review. *Food Science and Biotechnology*, 17(6), 1139-1145.
- Cornillon, P., & Salim, L. C. (2000). Characterization of water mobility and distribution in lowand intermediate-moisture food systems. *Magnetic Resonance Imaging*, 18(3), 335-341.
- Eerlingen, R. C., Jacobs, H., & Delcour, J. A. (1994). Enzyme-resistant starch. 5. Effect of retrogradation of waxy maize starch on enzyme susceptibility. *Cereal Chemistry*, 71(4), 351-355.
- Enrione, J. I., Hill, S. E., & Mitchell, J. R. (2007). Sorption and diffusional studies of extruded waxy maize starch-glycerol systems. *Starch-Starke*, *59*(1), 1-9.
- Gamble, G. R. (1994). Noninvasive determination of freezing effects in blueberry fruit tissue by magnetic-resonance-imaging. *Journal of Food Science*, *59*(3), 571-573.

- Himmelsbach, D. S., & Gamble, G. R. (1997). NMR, FT-IR, and FT-Raman spectroscopic imaging of grains. In: *International Workshop on Application of Magnetic Resonance and Other Spectroscopic Techniques to Food Science*.
- Hwang, S. S., Cheng, Y. C., Chang, C., Lur, H. S., & Lin, T. T. (2009). Magnetic resonance imaging and analyses of tempering processes in rice kernels. *Journal of Cereal Science*, 50(1), 36-42.
- Jouppila, K., & Roos, Y. H. (1997). The physical state of amorphous corn starch and its impact on crystallization. *Carbohydrate Polymers*, 32(2), 95-104.
- Kester, J. J., & Fennema, O. R. (1986). Edible films and coatings A review. *Food Technology*, 40(12), 47-59.
- Leung, H. K., Magnuson, J. A., & Bruinsma, B. L. (1983). Water binding of wheat-flour doughs and breads as studied by deuteron relaxation. *Journal of Food Science*, 48(1), 95-99.
- Lim, S., & Jane, J. (1994). Storage stability of injection-molded starch-zein plastics under dry and humid conditions. *Journal of Polymers and the Environment*, 2(2), 111.
- Mariette, F. (2009). Investigations of food colloids by NMR and MRI. *Current Opinion in Colloid & Interface Science*, 14(3), 203-211.
- Oztop, M. H., Rosenberg, M., Rosenberg, Y., McCarthy, K. L., & McCarthy, M. J. (2010).

 Magnetic Resonance Imaging (MRI) and Relaxation Spectrum Analysis as Methods to
 Investigate Swelling in Whey Protein Gels. *Journal of Food Science*, 75(8), E508-E515.
- Roca, E., Guillard, V., Guilbert, S., & Gontard, N. (2006). Moisture migration in a cereal composite food at high water activity: Effects of initial porosity and fat content. *Journal of Cereal Science*, 43(2), 144-151.

- Ruan, R., Almaer, S., Huang, V. T., Perkins, P., Chen, P., & Fulcher, R. G. (1996). Relationship between firming and water mobility in starch-based food systems during storage. *Cereal Chemistry*, 73(3), 328-332.
- Sievert, D., & Pomeranz, Y. (1989). Enzyme-resistant starch. 1. Chracterization and evaluation by enzymatic, thermoanalytical, and microscopic methods. *Cereal Chemistry*, 66(4), 342-347.
- Smits, A. L. M., Ruhnau, F. C., Vliegenthart, J. F. G., & van Soest, J. J. G. (1998). Ageing of starch based systems as observed with FT-IR and solid state NMR spectroscopy. *Starch-Starke*, *50*(11-12), 478-483.
- Whistler, R. L., & Daniel, J. R., eds (1985). *Carbohydrates in Food Chemistry*. New York: Academic Press.
- Zogzas, N. P., Maroulis, Z. B., & Marinoskouris, D. (1994). Moisture diffusivity methods of experimental determination A review. *Drying Technology*, 12(3), 483-515.

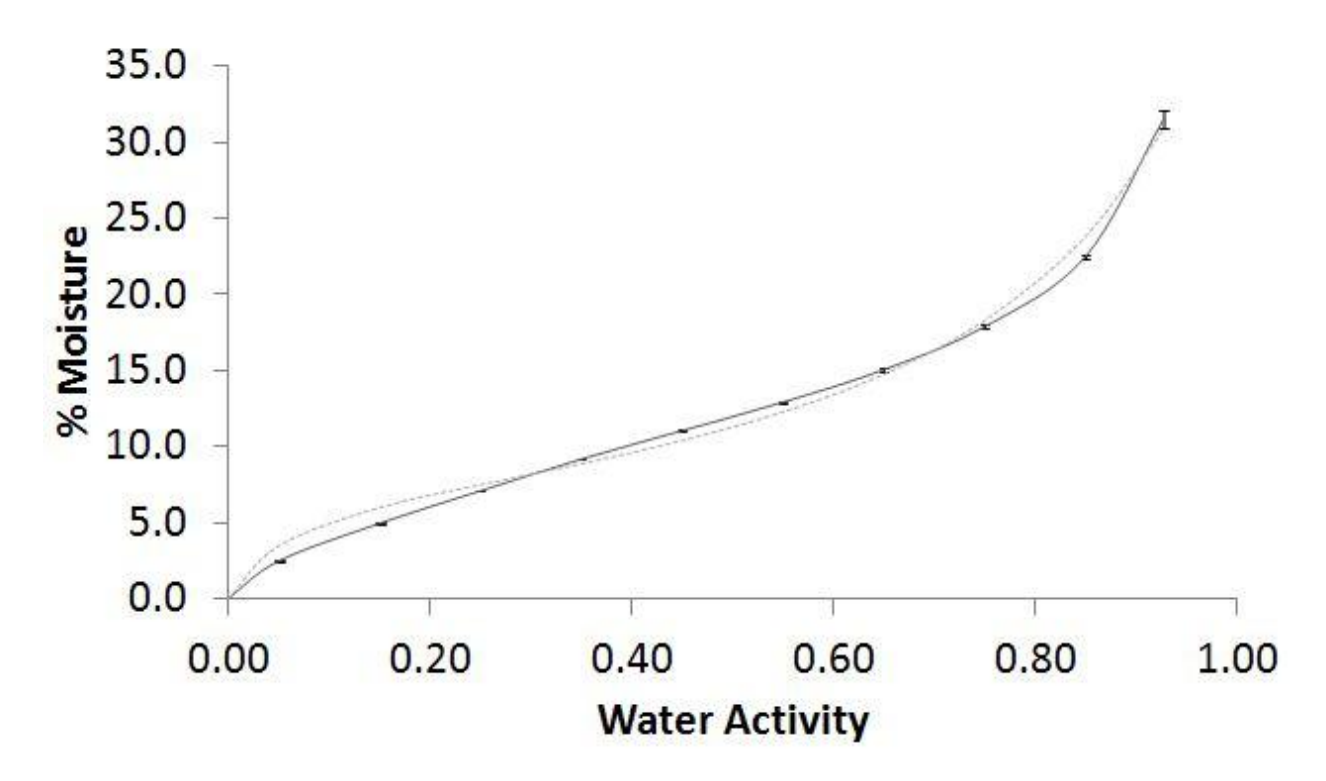


Figure 4.1. Sorption isotherm of starch extrudate. Solid line = IGASorp isotherm; Dashed line = GAB model of isotherm. Error bars are shown at each data point.

Table 4.1. Ratios of crystalline to amorphous starch peaks measured by FTIR

Treatment	Week of Storage	Crystalline:amorphous peak ratio (1037 cm ⁻¹ : 1014 cm ⁻¹)
	0	0.725±0.004
	2	0.718 ± 0.007
Full H ₂ O	4	0.736 ± 0.011
	8	0.727 ± 0.005
Half H ₂ O	0	0.725±0.004
	2	0.722 ± 0.001
	4	0.730 ± 0.006
	8	0.709 ± 0.009
Full D ₂ O	0	0.725±0.004
	2	0.739 ± 0.011
	4	0.740 ± 0.001
	8	0.748 ± 0.010
Half D ₂ O	0	0.725±0.004
	2	0.731 ± 0.003
	4	0.747 ± 0.011
	8	0.744 ± 0.003

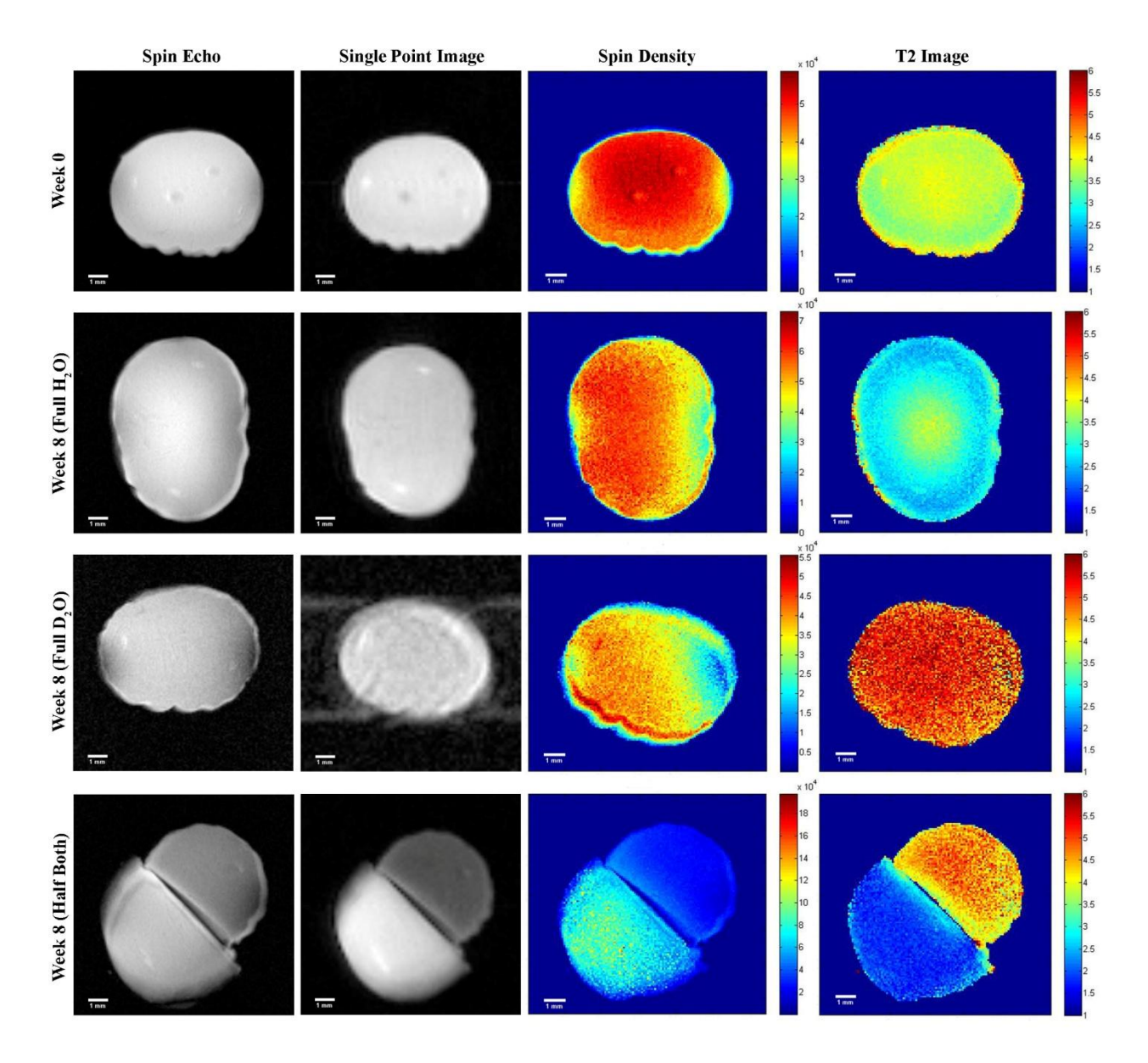


Figure 4.2. MRI images of starch extrudates. Spin Density image scales (Relative scale for each Spin Density image) to the right of the image color code the proton spin density. T2 Image scales (Same for all T2 images) to the right of the image color code the T_2 -relaxation times in milliseconds. Full H_2O = Intact extrudates (not bisected) stored in H_2O desiccator; Full D_2O = Intact extrudates (not bisected) stored in D_2O desiccator; Half Both = Bisected extrudates from both D_2O (top right) and H_2O (bottom left) desiccators. Scale bars = 1 mm.

Table 4.2. Description of methods used during MRI

Method	Type of water in image	Image Description	Can be compared to each other in this study?	Why / Why not?
Spin Echo (SE)	Free water only	Concentration and Mobility	No	Different sample lengths and imaging parameters
Single Point Imaging (SPI)	Free and bound water	Concentration	No	Different sample lengths and imaging parameters
Parameter- selective Spin Density (SD)	Free water only	Concentration	No	Different sample lengths, imaging parameters, and scales
Parameter- selective T2 (T2)	Free water only	Mobility (T ₂ -relaxation times)	Yes	Removes instrument and sample differences and compensates for different image parameters by using the same time scale

CHAPTER 5

CONCLUSIONS

This study showed several changes in the structure and moisture distribution in the starch extrudates during storage. The pore network within the extrudates increased in size and scope by the fourth week of storage, which may have been due to early stages of retrogradation or the migration of moisture throughout the extrudate. This change would allow for more moisture migration within the extrudate, which could lead to loss of quality. In addition, high density material of unknown composition was seen distributed throughout the sample with a higher concentration towards the center of the extrudate. The distribution of moisture in these extrudates changed drastically by the eighth week of storage. The complexity of the distribution of the free and bound water and the free water mobility suggests a probable relationship between the structural changes observed in these samples and the moisture migration during storage.

The use of Microcomputed tomography (microCT) to study starch extrudates provided new and interesting data concerning structural changes in these extrudates during storage. This technique provided 3-D images of the pore distribution and observed areas of higher density material as well as providing raw imaging data that was analyzed for a more in-depth study. The distribution of the structural changes observed in the extrudates during storage could not have been observed using analytical techniques and would have been difficult to obtain with other imaging techniques, which require extensive preparation of serial sections and destruction of the sample to provide similar information. MicroCT is a quick, non-destructive technique that

requires no preparation of the sample, making it an ideal imaging technique for extruded starch products.

The use of Magnetic Resonance Imaging (MRI) to study starch extrudates allowed imaging of the complex changes in moisture during storage. This technique showed the changes in the bound and free water distributions as well as the free water mobility. Analytical techniques could provide information about the free and bound water, but would not provide an image of the distribution throughout the extrudate. In addition, other imaging techniques are limited in their ability to produce images of moisture in a material and do not provide information about the mobility of the water. All of the imaging methods used in the MRI study provided useful information about the changes in the moisture distribution, but T2 imaging proved the most promising method for studying starch extrudates during storage because, unlike the other three methods used, the images can be compared to each other as long as the same time scale is used for the T2-relaxation times.

In conclusion, these imaging methods help to provide a better understanding of the changes occurring during storage of starch extrudates. The combination of these methods with more conventional analytical methods will provide a more complete understanding of changes affecting quality during storage, which could lead to extension of the shelf-life of these products. Future studies could focus on combining these methods with methods assessing texture differences and changes in physical properties to try to correlate observed structural and moisture changes with textural changes observed during loss of quality. In addition, future studies could focus on trying to determine the composition of the high density material within these extrudates by using differential staining with light microscopy.